Crack Initiation Analysis in Residual Stress Zones with Finite Element Methods

Patrick Joseph Brew

Thesis submitted to the faculty of Virginia Polytechnic Institute and State University in partial fulfillment of the requirements for the degree of

Masters of Science
In
Mechanical Engineering

Robert L. West, Chair

Norman E. Dowling

Reza Mirzaeifar

June 29th, 2018

Blacksburg, VA

Keywords: Fracture, Crack Initiation, Plastic Residual Stress Zones, Abaqus Submodeling, J-integral

Crack Initiation Analysis in Residual Stress Zones with Finite Element Methods

Patrick Joseph Brew

Academic Abstract

This research explores the nearly untapped research area of the analysis of fracture mechanics in residual stress zones. This type of research has become more prevalent in the field in recent years due to the increase in prominence of residual stress producing processes. Such processes include additive manufacturing of metals and installation procedures that lead to loads outside the anticipated standard operating load envelope.

Abaqus was used to generate models that iteratively advanced toward solving this problem using the compact tensile specimen geometry. The first model developed in this study is a two-dimensional fracture model which then led to the development of an improved three-dimensional fracture model. Both models used linear elastic fracture mechanics to determine the stress intensity factor (K) value. These two models were verified using closed-form equations from linear elastic fracture mechanics. The results of these two models validate the modeling techniques used for future model iterations. The final objective of this research is to develop an elastic-plastic fracture mechanics model. The first step in the development of an elastic-plastic fracture model is a three-dimensional quasi-static model that creates the global macroscale displacement field for the entire specimen geometry. The global model was then used to create a fracture submodel. The submodel utilized the displacement field to reduce the model volume, which allowed a higher mesh density to be applied to the part. The higher mesh density allowed more elements to be allocated to accurately represent the model behavior in the area local to the singularity. The techniques used to create this model were validated either by the linear elastic models or by supplementary dog bone prototype models. The prototype models were run to test model results, such as plastic stress-strain behavior, that were unable to be tested by just the linear elastic models. The elastic-plastic fracture mechanics global quasi-static model was verified using the plastic zone estimate and the fracture submodel resulted in a J-integral value.

The two-dimensional linear elastic model was validated within 6% and the three-dimensional linear elastic model was validated within 0.57% of the closed-form solution for linear elastic fracture mechanics. These results validated the modeling techniques. The elastic-plastic fracture mechanics quasi-static global model formed a residual stress zone using a Load-Unload-Reload load sequence. The quasi-static global model had a plastic zone with only a 0.02-inch variation from the analytical estimate of the plastic zone diameter. The quasi-static global model was also verified to exceed the limits of linear elastic fracture mechanics due to the size of the plastic zone in relation to the size of the compact specimen geometry. The difference between the three-dimensional linear elastic fracture model J-integral and the elastic-plastic fracture submodel initial loading J-integral was 3.75%. The J-integral for the reload step was 18% larger than the J-integral for the initial loading step in the elastic-plastic fracture submodel.

Crack Initiation Analysis in Residual Stress Zones with Finite Element Methods

Patrick Joseph Brew

General Audience Abstract

Additive manufacturing, sometimes referred to as 3-D printing, has become an area of rapid innovation. Additive manufacturing methods have many benefits such as the ability to produce complex geometries with a single process and a reduction in the amount of waste material. However, a problem with these processes is that very few methods have been created to analyze the initial part stresses caused by the processes used to additive manufacture.

Finite element methods are computer-based analyses that can determine the behavior of parts based off prescribed properties, shape, and loading conditions. This research utilizes a standard fracture determination shape to leverage finite element methods. The models determine when a crack will form in a part that has process stresses from additive manufacturing.

The model for crack initiation was first developed in two dimensions, neglecting the thickness of the part, using a basic material property definition. The same basic material property definition was next used to develop a crack initiation model in three dimensions. Then a more advanced material property definition was used to capture the impact of additive manufacturing on material properties. This material property definition was first used to establish the part properties as it relates to part weakening due to additive manufacturing. A higher accuracy model of just the crack development area was produced to determine the crack initiation properties of the additive manufactured part.

Methods previously confirmed by testing were used to validate the models produced in this research. The models demonstrated that under the same loading parts with initial processes stresses were closer to fracture than parts without initial stresses.

Acknowledgements

First, I would like to thank my committee chair, Dr. Bob West, for working with me over the past year and for preparing me for a future career in finite element development and fracture analysis. I would also like to thank my other committee members: Dr. Norman Dowling, whose class inspired me to pursue fracture mechanics as a career, and Dr. Reza Mirzaeifar, whose class first exposed me to finite element analysis.

I would also like to thank my mother, Cathleen Reilly, who supported me even when I made it difficult and has always sacrificed for my engineering passions and dreams. Additionally, I would like to thank my sister, Megan Brew, who always knew when I needed her to lift my spirits. Finally, I would like to thank my girlfriend, Sarah Busch, who was there for me every single day making sure that I stayed positive.

I would also like to thank the Center for the Enhancement of Engineering Diversity, especially Susan Arnold-Christian and Dr. Bevlee Watford, not only for providing me funding to pursue this research I am passionate about but also for being my family at Virginia Tech for the last five years.

Finally, I dedicate this thesis in honor of Steve Ruwe. He was my first FIRST robotics coach and without him I would not be an engineer. He passed away far too early this winter while volunteering with other young aspiring engineers. He is greatly missed but lives on through this work of mine and all the other students he mentored.

Contents

Academic Abstract…… ii

General Audience Abstract…….. iv

Acknowledgements……... v

Contents…… vi

List of Tables…… ix

List of Figures…… x

1.Introduction…… 1

1.1 Overview of the Project……...……. 1

1.2 Needs Statement…… 2

1.3 Hypothesis Statement…… 2

1.4 Goals and Objectives…… 3

1.5 Scope of Work…….. 4

2. Literature Review…….. 5

2.1 Finite Element Development for Fracture…… 5

2.2 Residual Stress State Development in Finite Elements…….. 10

2.3 Stress Intensity Factor Determination……. 12

3. Two-Dimensional Linear Elastic Model……... 15

3.1 Two-Dimensional Linear Elastic Finite Element Model Development……. 16

3.1.1 Two-Dimensional Part and partitioning Techniques……... 17

3.1.2 Two-Dimensional Material Properties……..... 18

3.1.3 Two-Dimensional Assembly and Interactions……. 19

3.1.4 Two-Dimensional Loads and Boundary Conditions……... 23

3.1.5 Two-Dimensional Mesh……... 25

3.2 Two-Dimensional Linear Elastic Finite Element Model Results……... 26

3.2.1 Stress and Energy Results for the Two-Dimensional Linear Elastic Model…… 26

3.2.2 Displacement Results for the Two-Dimensional Linear Elastic Model….. 28

3.2.3 Stress Intensity Factor Results for the Two-Dimensional Linear Elastic Model…… 29

3.3 Analytical Verification of Two-Dimensional Finite Element Model Results…… 30
4. Three-Dimensional Linear Elastic Model…… 33
4.1 Three-Dimensional Linear Elastic Finite Element Model Development……... 33
4.1.1 Three-Dimensional Part, Partitioning, and Material…… 34
4.1.2 Three-Dimensional Assembly and Interaction……... 36
4.1.3 Three-Dimensional Loads and Boundary Conditions…….. 37
4.1.4.Three-Dimensional Mesh……. 39
4.2 Three-Dimensional Linear Elastic Finite Element Model Results…… 41
4.2.1 Three-Dimensional Stress and Energy Results…… 41
4.2.2 Three-Dimensional Displacement Results……... 44
4.2.3 Three-Dimensional Stress Intensity Factor Results……. 45
4.3 Validation of Three-Dimensional Finite Element Model Results…….. 46
5. Three-Dimensional Plasticity Model…… 48
5.1 Quasi-Static Plastic Model Development……... 48
5.1.1 Quasi-Static Plastic Part and Partition……. 49
5.1.2 Quasi-Static Plastic Section and Material……..... 50
5.1.3 Quasi-Static Plastic Model Assembly and Interaction……..... 52
5.1.4 Quasi-Static Plastic Model Boundary Conditions……... 52
5.1.5 Quasi-Static Plastic Model Mesh……. 54
5.2 Quasi-Static Plastic Model Results and Verification…….. 55
5.2.1 Quasi-Static Plastic Far-Field Stress…… 55
5.2.2 Quasi-Static Plastic Model Plastic Zone Verification……. 57
5.3 Development of Refined Fracture Submodel……. 60
5.3.1 Fracture Submodel Attributes…….. 60
5.3.1 Fracture Submodel Part, Partition, and Material……. 61
5.3.3 Fracture Submodel Crack Properties……... 63
5.3.4 Fracture Submodel Boundary Conditions…… 65
5.3.5 Fracture Submodel Mesh……. 66
5.4 Results of Refined Fracture Submodel……... 67
5.4.1 Fracture Submodel Stress…… 68
5.4.2 Fracture Submodel J-integral……... 70

6. Summary, Conclusions, and Future Work……... 72
6.1 Goals and Objectives…….. 72
6.2 Summary of Completed Work and Conclusions…… 73
6.3 Future Work……..... 75
6.3.1 Future Model Improvements……..... 75
6.3.2 Expanded Capability to the Research…….. 75
6.3.3 Additional Applications for this Research……... 76
References…… 77
Appendix A: Ramberg-Osgood Material Law…… 79

List of Tables

3.1 Planar Dimensions for Two-Dimensional Linear Elastic Model……...…16

3.2 Radial Dimensions for Focus Partitions Local to Crack Tip…… 18

3.3 Elastic Material Properties for Aluminum 7075-T651……...….. 19

3.4 Two-Dimensional Linear Elastic Model Boundary Conditions ……..…24

3.5 Two-Dimensional Linear Elastic Model Load ……24

3.6 Reference Dimensions for Figure 3.1……31

4.1 Radial Dimensions for Focus Partitions Local to Crack Tip…….35

4.2 Three-Dimensional Linear Elastic Boundary Conditions ……38

4.3 Three-Dimensional Linear Elastic Loads ……....38

4.4 Summary of Stress Intensity Factors from Chap. 3 and Chap. 4 ……..….47

5.1 Nominal Plastic Tabular Aluminum 7075-T651 Data from Dowling E12.1…….....51

5.2 Top Pin Forced Displacement Loading Amplitude Tabular…….....53

5.3 Focus Area Partition Radii for Fracture Submodel……..……..62

List of Figures

2.1 Polar-plot type mesh strategy on a compact specimen ……..……..…….. 6

2.2 Midside node adjustment (red triangle linear elastic, blue square elastic- plastic)….. 7

2.3 Stress singularity function plot with midside node position highlighted…….....… 7

2.4 (a) Standard quadratic element. (b) Linear elastic degeneracy. (c) Elastic-plastic degeneracy……...…...… 8

2.5 Generalized stress-strain curve with unloading ……...…….. 10

2.6 Linear elastic fracture mechanics modes……..... 12

3.1 Normalized compact specimen dimensions from ASTM E399 [9]…….....….. 15

3.2 Compact specimen part geometry with partitioning……... 17

3.3 Contact property dialog box……..…….. 20

3.4 Abaqus interaction properties dialog box……..…… 21

3.5 Assembled model with all interactions shown…….……... 32

3.6 Crack front singularity properties Abaqus dialog window……. 23

3.7 Loads and boundary conditions on assembled model…….…… 24

3.8 (a) Full meshed assembly. (b) Focus mesh around crack front…….……. 25

3.9 Full model von Mises stress contour plot……..……. 27

3.10 Y-direction stress contours local to crack front…….....… 27

3.11 Elastic energy density contour plot……... 28

3.12 Displacement magnitude for two-dimensional model ……...…….....… 29

3.13 Key dimensions for closed-form solution……..……... 30

4.1(a) XY partitioning scheme. (b) YZ partitioning scheme…… 34

4.2 Three-dimensional compact specimen interactions……..……. 37

4.3 Three-dimensional compact specimen with loads and boundary conditions shown……...……. 39

4.4 Three-dimensional model colored by element type…….... 40

4.5 Meshed three-dimensional model…….**.....** 41

4.6 Y-direction stress zone around crack tip……..…….... 42

4.7 von Mises stress contour for full compact specimen……..… 42

4.8 Strain energy density contour plot…….. 43

4.9 Stress at crack tip YZ contour plot for half the thickness…….…….. 44

4.10 Displacement magnitude for full model …….……. 45

5.1 Partitioning scheme for plastic quasi-static model ……..……**..** 49

5.2 Top pin forced displacement loading amplitude plotted…….**.....** 53

5.3 Boundary conditions for quasi-static plasticity model……...……. 54

5.4 Mesh for quasi-static plastic model……...……. 55

5.5 von Mises stress contours at first full loading (*t*=0.32)……..…… 56

5.6 von Mises stress contours at full unloading (*t*=0.66)……..…..... 56

5.7 von Mises stress contours at second full loading (*t*=1.00)…….**.....** 57

5.8 von Mises contour of stress with lower limit of yield at the crack tip after one loading…….. 58

5.9 Contour of the plastic strain local to the crack tip after one load- unload cycle…….. 58

5.10 Submodeling attributes Abaqus dialog window…….……**..** 61

5.11 Cut submodel geometry for fracture analysis…….……**..** 62

5.12 Abaqus singularity dialog window settings for elastic-plastic fracture…….**.....** 64

5.13 Crack interaction for submodel……..…….. 64

5.14 Boundary condition for submodeling applied to new surfaces……. 65

5.15 Abaqus dialog window for submodel boundary condition……...……... 66

5.16 Fracture submodel mesh …….. 67

5.17 von Mises submodel stress contour plot for primary loading (*t*=0.32)……. 68

5.18 Submodel stress contour plot for unloading (*t*=0.66)……..……. 69

5.19 Submodel stress contour plot after reloading (*t*=1.00)……..…….... 69

5.20 Submodel plastic zone after complete unloading……. 70

1. Introduction

This introduction serves to provide a general background and motivation for the research detailed in the following sections. This section includes an overview of the project, the needs statement, goals and objectives for the work, and a discussion of the scope of the work.

1.1 Overview of the Project

This research seeks to develop and explore finite element modeling techniques to accurately model the behavior of crack initiation in plastic zones. There is no experimental data immediately available to validate the model. Therefore, the model needs to be robust in the methodologies and techniques used to create it. The modeling in this research focuses on the compact specimen geometry created in Abaqus. This research involves aspects of linear elastic fracture mechanics, elastic-plastic fracture mechanics, and finite element modeling to generate an accurate model, which accounts for the numerous challenges associated with this type of analysis.

The main challenge that drove the model refinement was the need for contour integrals to characterize the deformation around the crack tip so that the asymptotic behavior at the crack front is observable [1]. This issue is exacerbated by the unloading step, which leads to already deformed elements being further deformed. This study serves to determine methods that fracture can be modeled in a Load-Unload-Reload cycle so that the crack tip behaves as it does in load frame testing. Other challenges that occur when modeling fracture with finite elements are problems rectifying the free boundary condition in the area local to the crack front and the inability to grow the crack without remeshing. The remeshing for crack growth issue is not pertinent to the work in this research because this research focuses solely on fracture initiation.

1.2 Needs Statement

As the usage and innovation in additive manufacturing has increased, the methods for analyzing parts produced by additive manufacture processes have not developed at the same rate. Previously, there were no published methods for fracture mechanics in residual stress zones as it related to metallic additive manufactured components. While this work does not directly deal with the processes involved with additive manufacture, the application of the same modeling techniques are valid for those processes. This analysis can also be used in applications that experience loads outside the anticipated operating envelope during installation procedures or other operating conditions that cause the material to enter the plastic region, making the part susceptible to fracture initiation.

Cain et al [2] wrote that there was a need for improvement to reduce the costs of performing research that characterizes the properties of specimen made by additive manufacturing. The study Cain performed involved printing hundreds of specimen in different orientations and testing them experimentally which was expensive, time consuming, and limited in scope. A robustly developed finite element model could relieve the cost burden and create techniques to model any geometry or print orientation.

1.3 Hypothesis Statement

A robust model for crack initiation in a plastic zone can be produced through an iterative model development approach. The first models in this approach will validate modeling techniques that are shared with linear elastic fracture mechanics. These techniques include meshing strategy, geometry, and load development. The linear elastic models, first two-dimensional then three-dimensional, will be validated using stress intensity factor closed-form solutions rooted in linear elasticity [3]. Once the linear elastic models are validated, the techniques developed will be used as the starting point for the elastic-plastic modeling step. This step will also incorporate results from supplementary dog bone models that are designed to verify the plastic stress-strain behavior of the material and the submodeling techniques. Once

the dog bone models are verified, a global model for the elastic-plastic fracture mechanics condition is created. The global model is verified to first ensure the plastic zone diameter is reasonably close to the closed-form estimate [3] and second to ensure that the model exceeds the limits of the linear elastic fracture mechanics assumptions. Finally, a fracture submodel is developed and the J-integral is computed from a smaller section of geometry. This model is robust enough that the resulting J-integral is a reasonable value for the load case.

1.4 Goals and Objectives

The main goal of this study is to produce a set of iterative models that support finite element model development to perform fracture initiation analysis in a plastic zone. The supporting iterative models are the two and three-dimensional linear elastic fracture models. Another goal is to have both linear elastic models adequately fit the closed-form linear elastic fracture mechanics solutions. This fit will verify the accuracy of the models and validate the techniques used in their development. Models to verify the plastic material properties, the behavior of submodels, and the plastic zone in a fracture model must also be produced to validate the aspects of the elastic-plastic fracture model that are not able to be validated by the linear elastic models. The explicit objectives required to obtain the goals discussed above are enumerated below:

1. Model linear elastic fracture mechanics to be used in validating the meshing scheme and modeling techniques,
2. Validate linear elastic compact specimen models with the linear elastic closed-form solution,
3. Validate modeling techniques for elastic-plastic model that are not validated by the linear elastic models using supplementary dog bone prototype models,
4. Develop methods for creating a plastic zone by elastic-plastic response around the crack tip,

5. Develop methods for transferring stresses from a quasi-static model with a plastic zone to a fracture model,
6. Model elastic-plastic fracture mechanics for a compact specimen.

1.5 Scope of Work

The scope of this work is well defined and has clear limitations. This research only examines crack-opening fracture (Mode I) and all other forms are shown to be negligible. Only examining Mode I is justified since the models show the other modes are orders of magnitude smaller and because the compact tensile specimen geometry is designed to isolate Mode I. The only geometry investigated in this study is the compact tensile specimen. The compact tensile specimen is the typical specimen used to determine fracture properties to characterize a material. Therefore, the results of this research can be extrapolated to any other geometry. No experiments will be conducted nor will any experimental data be referenced in this research. This scope refinement is due to the existence of already developed closed-form solutions for linear elastic fracture mechanics that can be used in model validation and the dearth of accurate information about experimental plastic cyclic loading to generate a residual stress.

2. Literature Review

This chapter serves to summarize the published literature pertinent to the work conducted in this research. The main objective areas explored during this research were:

1. Finite element model development for fracture,
2. Residual stress state development in finite element modeling,
3. Stress intensity factor determination.

The review of the current literature in these objective areas enables the development of a residual stress fracture model that utilizes the most up to date methods.

2.1 Finite Element Development for Fracture

The literature suggests that any finite element model whose purpose is to capture fracture data needs to be specifically tailored to obtain that data. The challenge with meshing a crack is that the crack front is represented by a singularity, which can provide computationally unstable results in the local region. The prevailing technique in the literature to prevent the instability of the crack tip is to develop a focus mesh at the crack tip. This specialized focus mesh employs a partitioning strategy that generates a polar-plot type mesh in the local area to the crack tip. The benefit of using this meshing scheme is there are constant radius elements for the contour integrals to be taken around. The optimal sweep angle for the polar-plot mesh is between 12 and 22 degrees. An example of this meshing strategy is shown below in Fig. 2.1 [4].

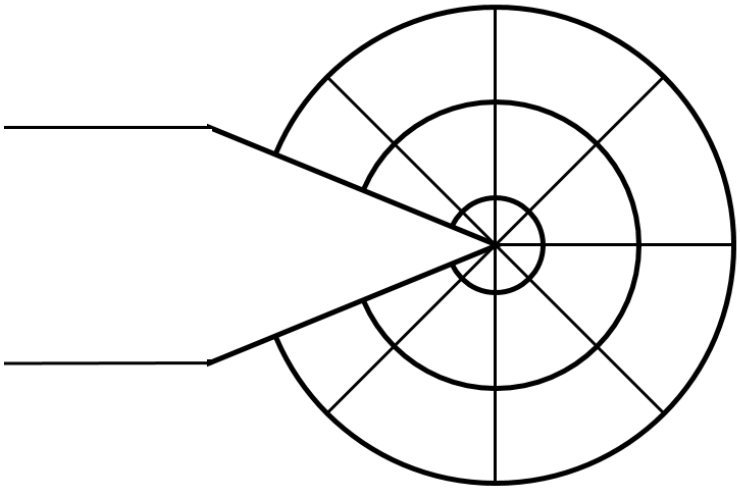

Figure 2.1 Polar-plot type mesh strategy on a compact specimen.

Additional adjustments are needed to best construct the elements closest to the crack front so that they are capable of capturing the behavior at the singularity. These methods include modifying the position of the midside node [5] and collapsing one side of the element at the crack tip to form a degenerate element at the singularity [6].

Linear elastic fracture mechanics models have the midside node moved to the quarter point nearest to the crack front. This manipulation is done to capture the assumed $\frac{1}{\sqrt{r}}$ stress singularity behavior at the crack front. This assumption is only valid when the plastic zone is significantly small; meaning small scale yielding theory is valid. Elastic-plastic fracture mechanics models leave the midside node in the middle of the element to obtain the $\frac{1}{r}$ stress singularity at the crack front. The manipulation of the midside node is shown in Fig. 2.2 below.

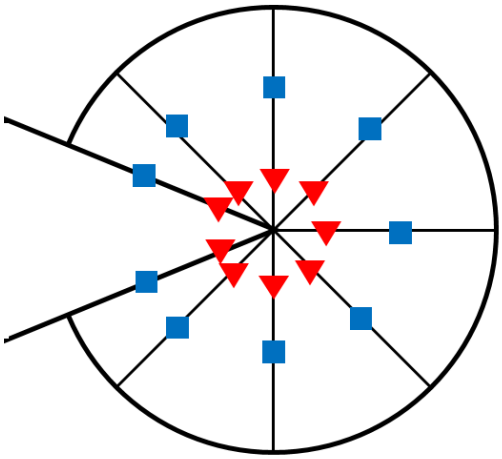

Figure 2.2 Midside node adjustment (red triangle linear elastic, blue square elastic-plastic).

A plot of the stress singularity functions for both linear elastic and elastic-plastic fracture mechanics are shown below in Fig. 2.3. The midside node location is highlighted with a point on both curves.

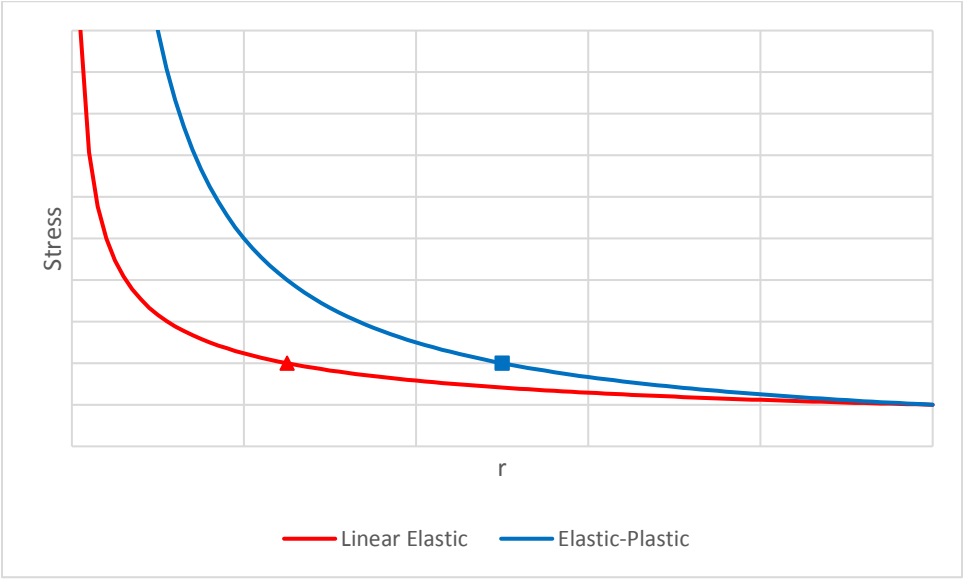

Figure 2.3 Stress singularity function plot with midside node position highlighted.

The second adjustment needed at the crack front is determining the degeneracy method for the element at the crack tip. For linear elastic fracture mechanics, the nodes in a quadratic element on the collapsed side are combined into a single node resulting in a $1/\sqrt{r}$ singularity. For elastic-plastic fracture mechanics, the nodes of the quadratic element are duplicated at the same location, resulting in a $1/r$ singularity. The node collapsing process is show below in Fig. 2.4.

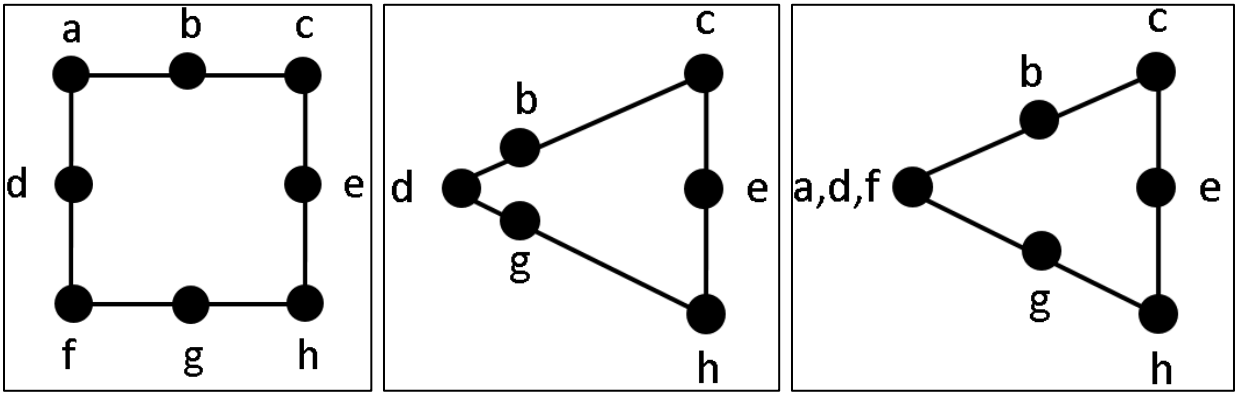

Figure 2.4 (a) Standard quadratic element. **(b)** Linear elastic degeneracy. **(c)** Elastic-plastic degeneracy.

The reason that the degeneracy is handled differently for linear elastic fracture and elastic-plastic fracture is due to the singularity at the crack tip. The strain vs. radius functional relationship that supports this adjustment is shown in Eqn. 2.1.

$$\varepsilon \to \frac{A}{r} + \frac{B}{\sqrt{r}} \; as \; r \to 0 \tag{2.1}$$

When the nodes are combined, and therefore constrained to move together, in the linear elastic case *A*=0. When the nodes are free to move independently of each other in the elastic-plastic case *B*=0. When either of these conditions is applied to Eqn. 2.1 the resulting relationship

is the function for the strain singularity that satisfies the condition for either the linear elastic or elastic-plastic method of fracture mechanics [1].

In three-dimensional fracture mechanics models, either 20 or 27 node quadratic elements may be used at the crack front. Similar to the midside node adjustment in two-dimensions, the midside node is moved to the quarter point for linear elastic models and remains in the middle for elastic-plastic models. The only exception is that the centroid node is unable to be moved in the three-dimensional fracture model. This causes the J-integral at the midplane of the element to vary from the J-integral at the edge plane of the element. These variations are generally small but should be kept in mind when deciding on a through-thickness meshing scheme. The meshing scheme should have an edge plane at the through-thickness location of highest interest.

Element selection and shape plays a large role in the accuracy of finite element models for fracture. Element edges should be straight and any plane perpendicular to the crack front should be flat. Additionally, it is most effective to use sweep meshing at the crack tip to ensure constant meshing through the thickness of the part. The most effective elements to use around a crack tip are second-order, also known as quadratic elements, using a reduced integration scheme. Quadratic elements must be used because the quadratic interpolation functions with the midside node adjustment are able to adequately represent the singularity, linear elements do not have the midside node. Reduced integration elements are preferred for fracture applications because full integration methods move the Gauss point, also called the integration point, too close to the crack front. The repositioning of the midside node in linear elastic fracture mechanics also repositions the integration point for the element. The integration point nearest the crack front is moved too close to the singularity and can produce unstable results in a full integration scheme. Hybrid integration methods are optional when the Poisson's ratio is less than 0.5 but can help with convergence around the crack tip [1]. The Poisson's ratio for the material used in the linear elastic modeling sections of this research is well below 0.5 so the use of hybrid elements is optional. Plastic zones are considered to be incompressible and have a Poisson's ratio of 0.5. Using hybrid elements adds a Lagrange multiplier to the element formulation to enforce the incompressibility constraint and can increase computational expense. The elements in the elastic-plastic fracture mechanics model that comprise the plastic region must use the hybrid formulation.

2.2 Residual Stress State Development in Finite Elements

Another objective area for this research is determining the residual stress states of materials when they are loaded cyclically. There are numerous methods by which residual stress states are capable of being developed such as thermal gradients, manufacturing processes, or material phase changes. However, this study will focus on residual stress states caused by elastic-plastic response. One way to explore this topic is through investigating the stress-strain curve for a material that is loaded and then fully unloaded. The generalized complete load-unload stress-strain curve shown in Fig. 2.5 demonstrates why the material properties are changed in a residual stress zone [3].

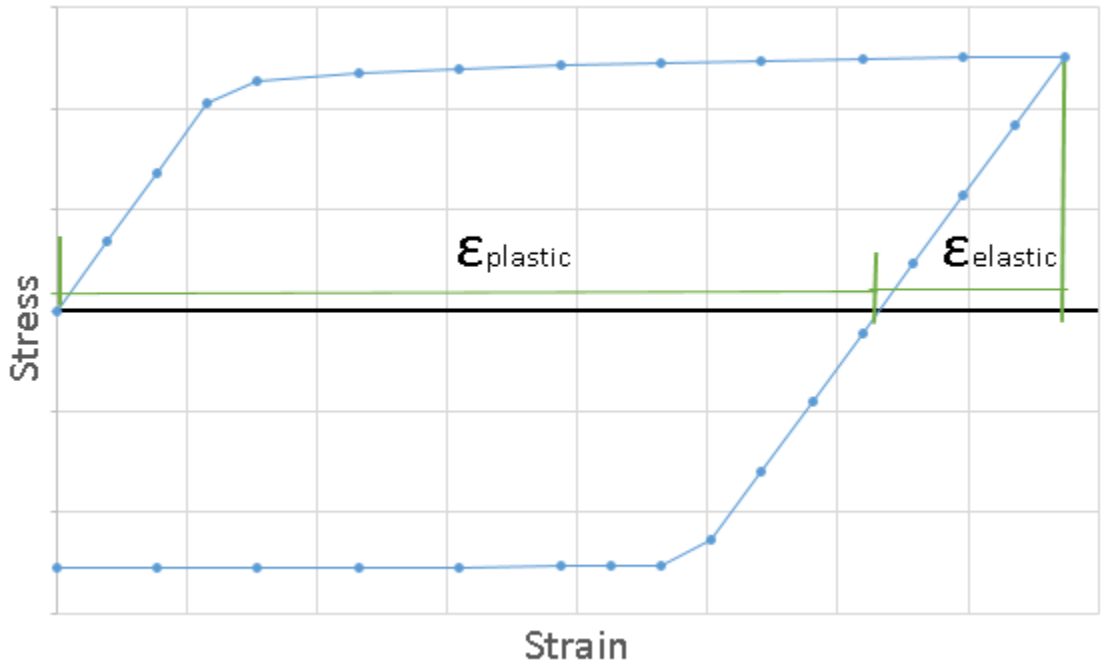

Figure 2.5 Generalized stress-strain curve with unloading.

Starting at zero stress and zero strain the stress grows proportionally to the strain in the linear elastic region. The constant of proportionality is Young's Modulus. The loading is

completely reversible and the unloading follows the original loading path in the elastic region. When the load exceeds the yield point the stress-strain response transitions into the plastic region. The plastic region stress-strain relationship is no longer a linear relationship with the Young's Modulus of the material as the slope. Moreover, strain accumulated in this region is not elastically reversible. As shown in Fig. 2.5 the elastic strain accumulated in the elastic region is unloaded down a line parallel to the elastic loading region while the plastic strain is constant throughout unloading. Two times as much elastic unloading as elastic loading must be performed before the material begins to unload plastically [3]. The equation for total strain is shown in Eqn. 2.2 below.

$$\varepsilon_{Total} = \varepsilon_{elastic} + \varepsilon_{plastic} \tag{2.2}$$

The stress-strain curve through full strain unloading ($\varepsilon_{Total}=0$) is shown in Fig. 2.5. The models developed in this research never meet the plastic unloading condition because of the geometry of the compact specimen and the load profile.

The plastic zone in the compact specimen is generated by the elastic-plastic response discussed in this section. The loading for the models in this research causes the region around the crack front to deform plastically. Then, during unloading, the rest of the compact specimen away from the crack front returns elastically to a zero stress- zero strain state while the region around the crack front still has plastic strain. This remaining plastic strain forms the plastic zone residual stress ahead of the crack front.

Abaqus has numerous methods for producing a plastic material property including using tabular data and importing a Ramberg-Osgood property curve. The Ramberg-Osgood approach is discussed in more detail in Appendix A. The tabular data approach relies on having stress and plastic strain experimental data available for the given material. Once the data points are collected, they are input into the plastic material property.

2.3 Stress Intensity Factor Determination

The stress intensity factor in these models is defined in two separate ways: one for linear elastic fracture mechanics and another for elastic-plastic fracture mechanics. For linear elastic fracture mechanics, the stress intensity factor K is used. A K value exists for each of the three linear elastic fracture modes. The three linear elastic facture modes are opening (Mode I), sliding (Mode II), and tearing (Mode III). The different linear elastic fracture modes are shown below in Fig. 2.6.

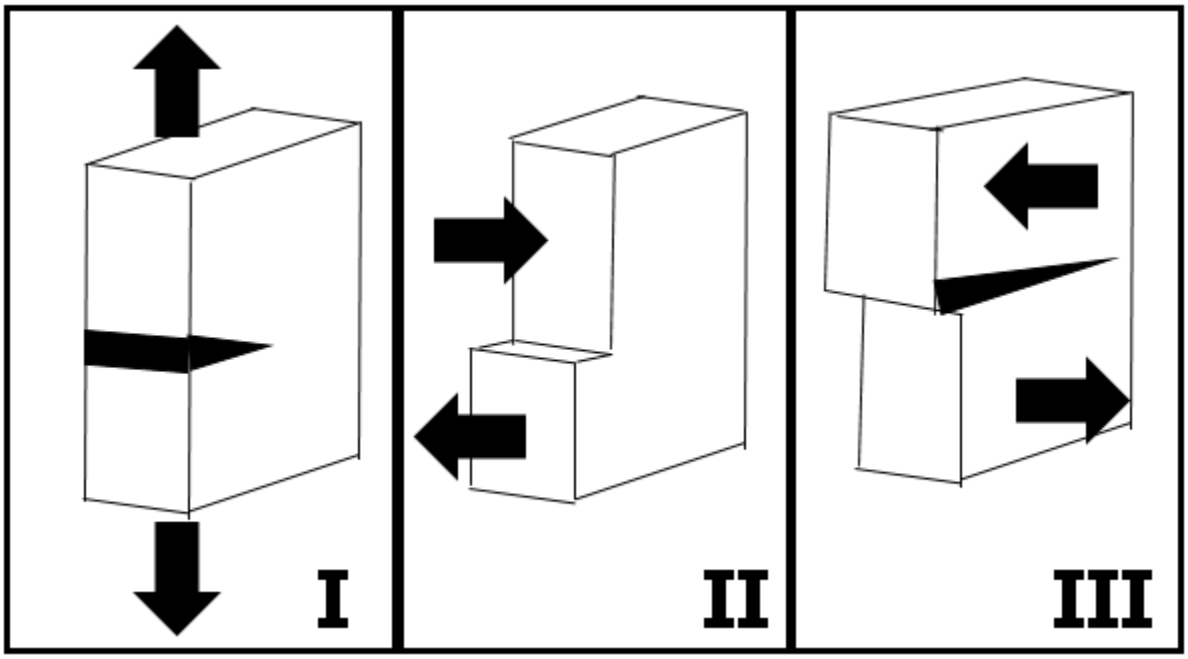

Figure 2.6 Linear elastic fracture mechanics modes.

The linear elastic stress intensity factor in the Mode I direction generally behaves according to Eqn. 2.3 below [3].

$$K_I = \lim_{r,\theta \to 0} (\sigma_y \sqrt{2\pi r}) \tag{2.3}$$

K_I is the stress intensity factor for Mode I fracture, σ_y is the directional stress causing the opening mode fracture, r is the distance from the crack front, and θ is the angle from the crack front. Equation 2.3 holds true for all linear elastic fracture mechanics problems. Often, Eqn. 2.3 is expressed as a closed-form equation specific to the geometry and loading of the crack.

K_I is valid for linear elastic fracture mechanics. In elastic-plastic fracture mechanics models, the J-integral is used for determining the stress intensity. The J-integral is a metric based on energy so it can be used for both linear elastic fracture mechanics and elastic-plastic fracture mechanics. The J-integral is a path independent method for determining the rate of change of the potential energy with respect to crack length growth [7]. The equation for the J-integral is shown below in Eqn. 2.4.

$$J = -\left(\frac{du_M}{da}\right) = \int_s (w dy - T \cdot \frac{du}{dx} ds) \tag{2.4}$$

McMeeking studied elastic-plastic fracture mechanics as it related to notched crack fronts in opening mode fracture [8]. This study validates Baroum's finite element mesh midside node adjustment and practically applies Rice's J-integral approach to fracture energy to a finite element approach. This study's validation of these methods in an elastic-plastic fracture mechanics application demonstrates this approach's worthiness for use in this research's ensuing steps. This study does not explore any residual stress states; however, a single monotonic plastic loading is applied to a notched specimen loaded into the plastic region.

Linear elastic fracture mechanics has methods for relating the J-integral to the K stress intensity factor. Equations 2.5, 2.6, and 2.7 demonstrate the relationship.

$$J = G \tag{2.5}$$

$$G = \frac{K^2}{E'} \tag{2.6}$$

$$E' = E\ (plane\ stress;\ \sigma_z = 0) \qquad (2.7)$$
$$E' = \frac{E}{1-\nu^2}\ (plane\ strain;\ \varepsilon_z = 0)$$

The equations above define *E* as Young's Modulus and *v* as Poisson's ratio [3]. This equation can be used to relate a J-integral value for a linear elastic fracture mechanics problem to a stress intensity, K_I, which in turn can be compared to a fracture toughness value, K_{Ic}.

The fracture toughness value, K_{Ic}, is directly compared with a K_I stress intensity value to determine if fracture initiation will occur according to Eqn. 2.8.

$$K_I \geq K_{Ic} \quad Fracture\ Intiates \qquad (2.8)$$
$$K_I < K_{Ic}\ No\ Fracture\ Intiation$$

Fracture toughness is a material property determined by ASTM E399, which can be used in linear elastic fracture mechanics. A relationship similar to Eqn. 2.13 exists between J and J_{Ic} to determine if fracture initiates in non-linear elastic mode one fracture problems.

3. Two-Dimensional Linear Elastic Model

The first step toward the exploration of this topic is to develop a basic modeling technique for fracture mechanics in Abaqus. The technique was verified by comparing the results of the model against analytical methods of computing the stress intensity factor, K_I. To achieve this, a compact specimen finite element model estimate of K_I was verified against the analytical solution for the compact specimen stress intensity factor [3]. Both the finite element model and the analytical model seek to replicate the behavior that a physical compact specimen would experience if being tested in a load frame.

A diagram of the shape and normalized dimensions for the compact specimen, as specified in ASTM E399, is shown below in Fig. 3.1.

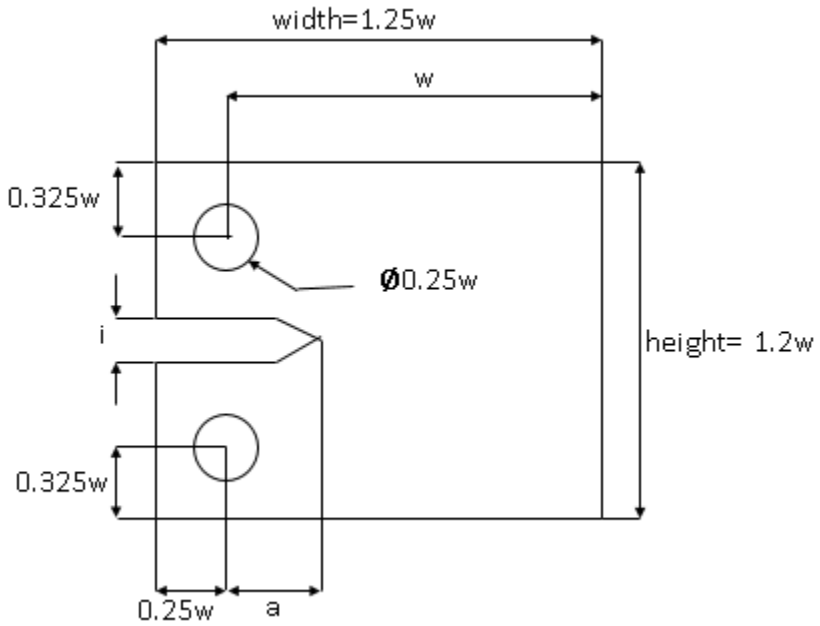

Figure 3.1 Normalized compact specimen dimensions from ASTM E399 [9].

The main components of this load geometry are the holes and the crack tip inlet. The holes allow the load frame to apply displacements to the specimen and the inlet provides a stress

raiser to encourage crack initiation and growth from the sharp tip. For this study, the parameter *w* = 2 inches. This created an overall specimen footprint that was 2.5 inches wide and 2.4 inches in height. Additionally, in the finite element and analytical models of this fracture geometry, the initial crack length, *a*, was set to the tip of the sharp inlet. Two additional important dimensions for the compact specimen used in this study are 0.125 inches for the inlet opening height and 0.4 inches for the sharp tip distance from the center of the machine connection holes. A summary of the planar dimensions used in this chapter is provided in Table 3.1.

Table 3.1 Planar Dimensions for Two-Dimensional Linear Elastic Model

Parameter	**Length (in)**
w	2
a	0.4
i	0.125
Height	2.4
Width	2.5

Each of the subsequent subchapters details the development of the finite element model, the results of the finite element model, and the results of the analytical calculation for the compact specimen fracture geometry.

3.1 Two-Dimensional Linear Elastic Finite Element Model Development

A two-dimensional model was constructed with the compact specimen dimensions as specified in Fig. 3.1 and Table 3.1. This section is dedicated to the discussion of the development methods used for creating the two-dimensional linear elastic fracture mechanics model.

3.1.1 Two-Dimensional Part and Partitioning Techniques

The geometry was generated in Abaqus using a 2D planar modeling space and a *Deformable* type. This allows for the cross sectional sketch to be assigned a depth in the section assignment. Partitions were added to the compact specimen geometry to provide advantages during the meshing process as shown below in Fig. 3.2.

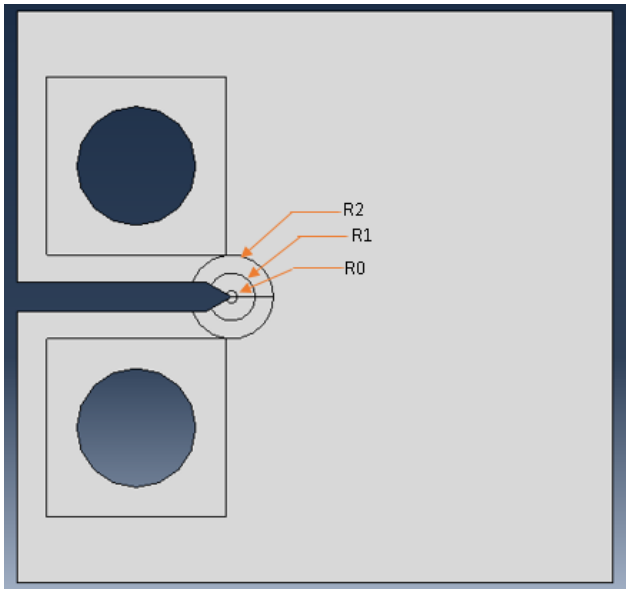

Figure 3.2 Compact specimen part geometry with partitioning.

The square partitions around the machine interface holes allow proper meshing of the holes. This is essential to the accuracy of the model because this is how the load is transferred from the load frame through the actuated pin, then through the material and is reacted by the fixed pin. The load transfer causes deformation that develops strain energy along the load path including at the sharp tip of the inlet where the crack front is located. The three circular partitions around the sharp tip of the compact specimen inlet are to provide an adequate focus

mesh around the crack tip. The focus mesh partition circles, in conjunction with the single line partition connecting each concentric circle partition to the crack tip, provide the polar-plot type mesh as discussed in Chap. 2.1. The radii for each of the partitions in the crack tip focus area is shown in Table 3.2.

Table 3.2 Radial Dimensions for Focus Partitions Local to Crack Tip

Partition	Radius (in)
R0	0.025
R1	0.1
R2	0.175

The smallest partition circle, R0, serves the purpose of ensuring that the first element is correctly capturing the singularity at the crack front. The next smallest partition, R1, has a radius of 0.1 inches and it is responsible for generating the elements that are used for computing the remaining contour integrals. The largest partition of the crack tip focus area, R2, intersects with the machine pinhole focus area boundary partition tangentially to ensure that there is a path of high mesh density for load transfer into the crack tip region.

Additionally, a 2D planar part was created of type *Analytical Rigid* to simulate the pins that connect the load frame to the compact specimen. The *Analytical Rigid* type is used in this model to provide a contact surface to represent the connection to the load frame without needing to be meshed. *Analytical Rigid* parts maintain their shape and are controlled by a single reference point, for the pin part it is located at the center of the circular pin [10]. An *Analytical Rigid* pin is acceptable for use here because the pins are made of hardened tool steel which when in contact with the aluminum compact specimen experiences negligible deformations.

3.1.2 Two-Dimensional Material Properties

The material used in this model is Aluminum 7075-T651, which has a high strength to weight ratio making it commonly used in transportation applications such as aerospace and automotive as well as in high-end performance consumer products [11]. Only elastic properties were necessary for this model and the material was considered completely isotropic with material properties as shown in Table 3.3.

Table 3.3 Elastic Material Properties for Aluminum 7075-T651

Parameter	**Value**
Young's Modulus (E)	10.3×10^6 psi
Poisson's Ration (ν)	0.33

This material property was utilized to create a section property with a depth of 0.125 inches that was then assigned to the entire compact specimen part.

3.1.3 Two-Dimensional Assembly and Interactions

The model is assembled using coincident constraints to mate the center of the compact specimen's pinholes to the center reference point of the rigid analytical machine pins. Additionally, interactions are established between the pins and the holes for both the top and bottom pin positions. Each interaction is established using the finite sliding method with slave adjustment only to remove overclosure and no surface smoothing performed. Figure 3.3 shows the Abaqus dialog window to set this interaction.

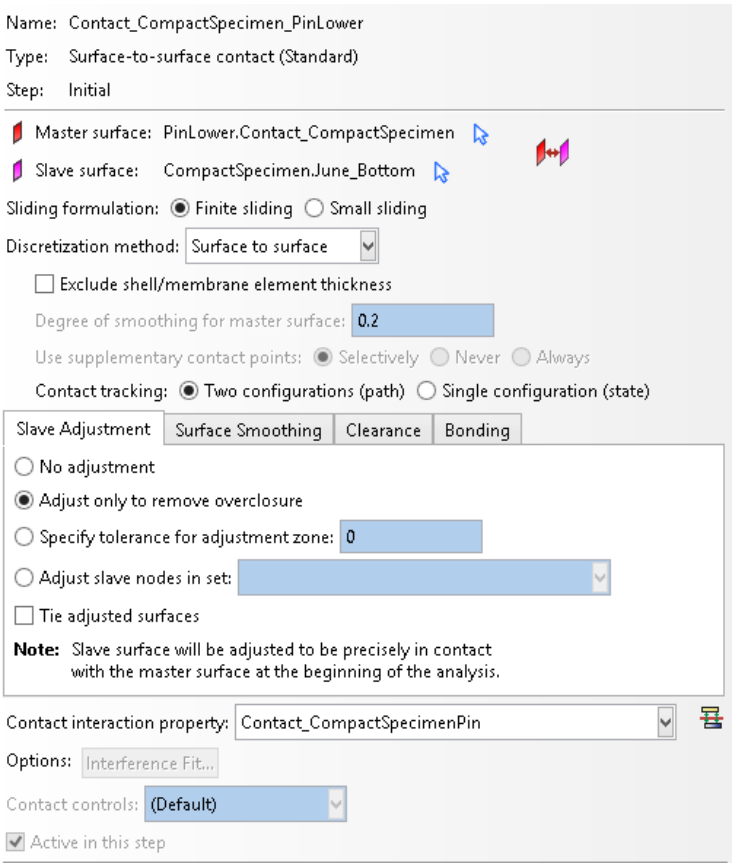

Figure 3.3 Contact property dialog box.

The *Rigid Analytical* pin acts as the master surface by definition. The compact specimen hole behaves as the slave surface because the hole in the specimen will be the part of the interaction that will be deforming. Both the top and bottom pins are defined with the same contact property that states that in the tangential direction there shall be penalty-based friction with a coefficient of 0.61. This is the friction coefficient between a hardened tool steel and aluminum [12]. The interaction property states that in the normal direction there shall be hard contact with a penalty method that behaves linearly with a stiffness scale factor of one and no clearance when the contact pressure is zero, however, separation is allowed after contact. The contact is established in the initial step and is then propagated to the subsequent loading step. Figure 3.4 shows the Abaqus dialog box settings for generating this interaction property.

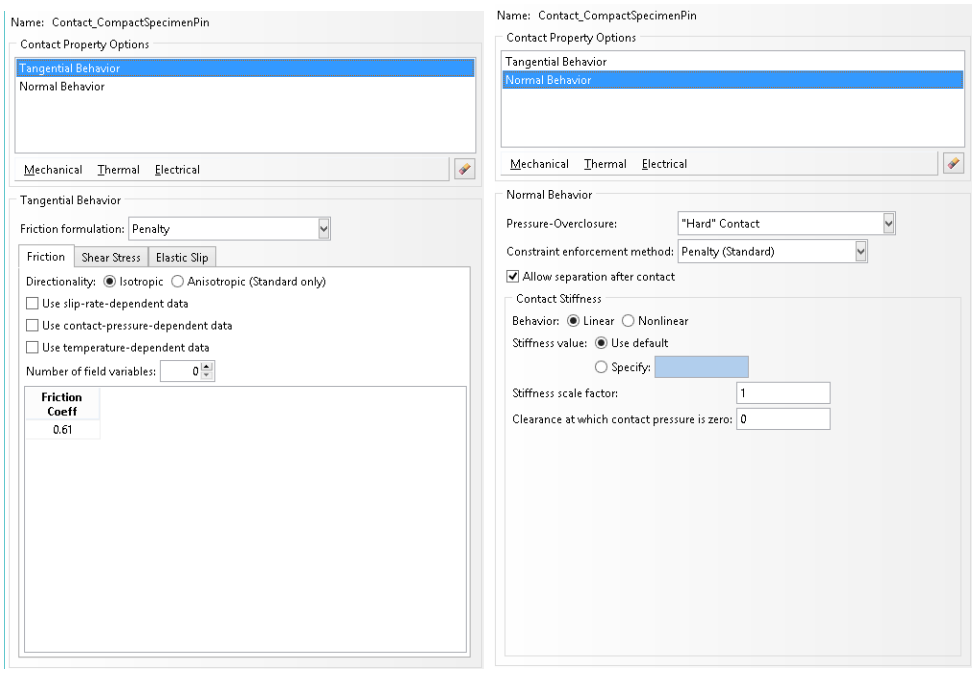

Figure 3.4 Abaqus interaction properties dialog box.

The crack is defined in the same module as the interactions. In this model, the crack tip is located directly at the sharp tip of the compact specimen inlet. The q-vector, a direction cosine used to define the crack extension direction, is (1,0,0). The q-vector is shown in Fig. 3.3 in blue and the crack tip is demarcated with a green “X”.

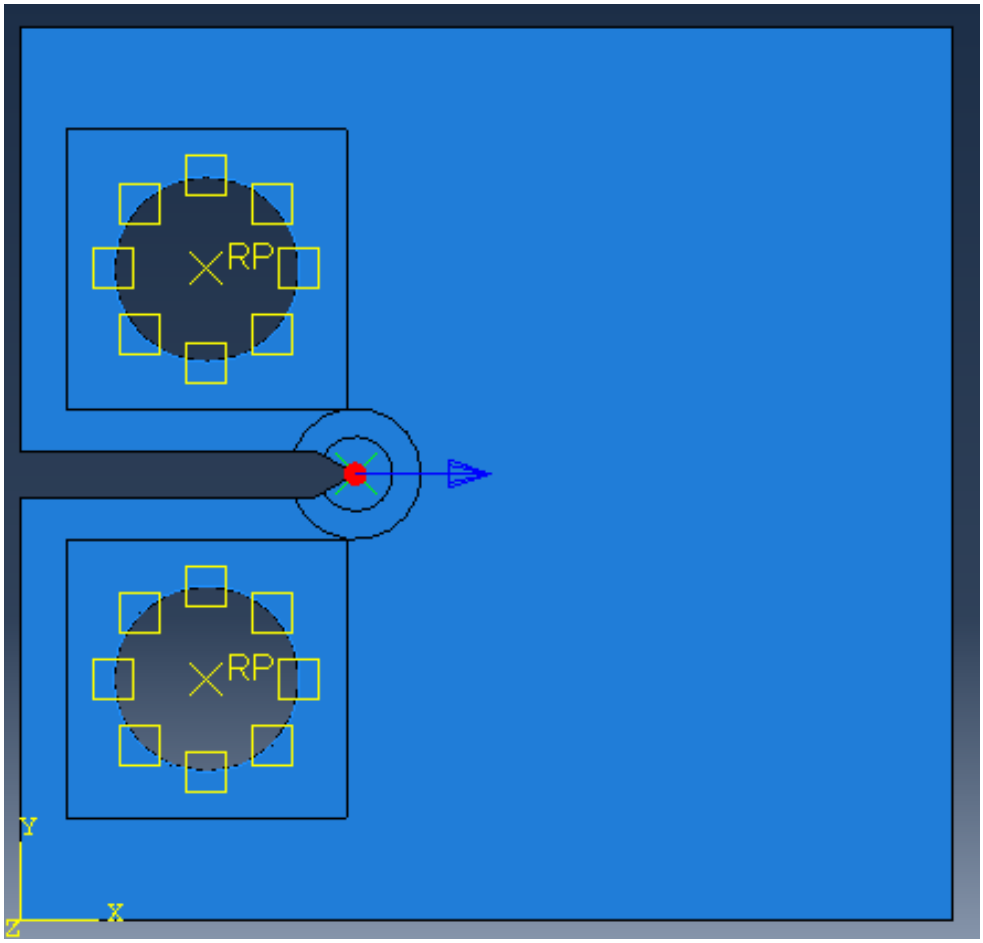

Figure 3.5 Assembled model with all interactions shown.

The crack has additional properties to characterize the singularity at the crack tip. First, the midside node is moved to the quarter point of the model to better capture the linear elastic fracture behavior that has a singularity proportional to $\frac{1}{\sqrt{r}}$. The elements at the crack tip have one side of the quadrilateral element collapsed to capture the linear elastic fracture behavior completely. The nodes that are impacted by the degeneration of one side of the element are replaced with a single node. The Abaqus dialog window to generate the crack front singularity mesh properties is shown below in Fig. 3.6.

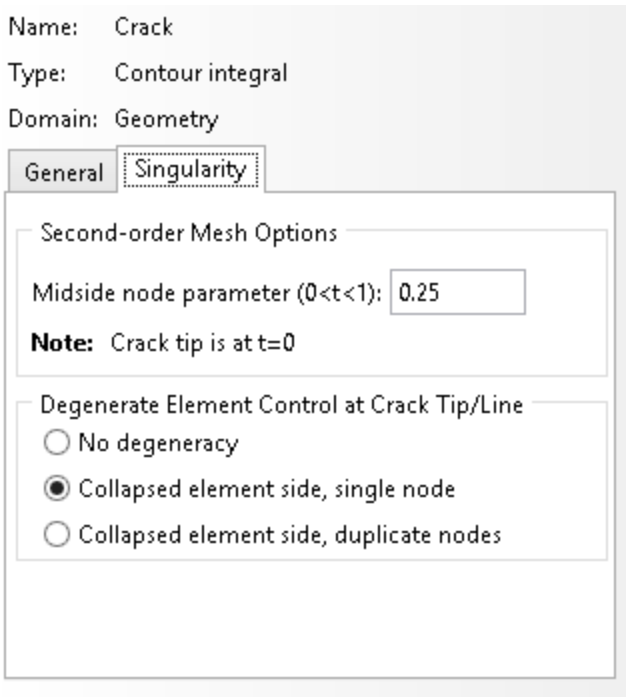

Figure 3.6 Crack front singularity properties Abaqus dialog window.

3.1.4 Two-Dimensional Loads and Boundary Conditions

Load and boundary conditions for this model are solely applied to the reference points of the rigid machine pins. A fixed boundary condition is applied to the bottom pin in the initial step, which remains in place while the top pin is loaded. The top pin in a universal load frame experiment would be held fixed while the bottom pin would be actuated. Switching which pin is actuated and which is fixed for this model has no impact on the stress intensity factor results that the model is designed to produce. In the loading step, the top pin has a boundary condition applied to it that prevents it from rotating or moving in the X-direction. The boundary condition applied to the top pin replicates the load frame test where the actuated pin is only able to move along the Y-axis. The boundary conditions for this model are shown in Table 3.4 below.

Table 3.4 Two-Dimensional Linear Elastic Model Boundary Conditions Table

Location	Boundary Condition
Bottom Pin	U1=U2=U3=UR1=UR2=UR3=0.0
Top Pin	U1= U3=UR1=UR2=UR3=0.0

Moreover, in the loading step the top pin has a concentrated force of 1,000 lbf applied at the reference point and in the Y-direction. This load represents a load-controlled experiment. The loading for this model is shown in Table 3.5 below. Figure 3.7 below Table 3.5 shows the load applied to the assembled model.

Table 3.5 Two-Dimensional Linear Elastic Model Load Table

Location	Load
Top Pin	CF2=1,000 lbf

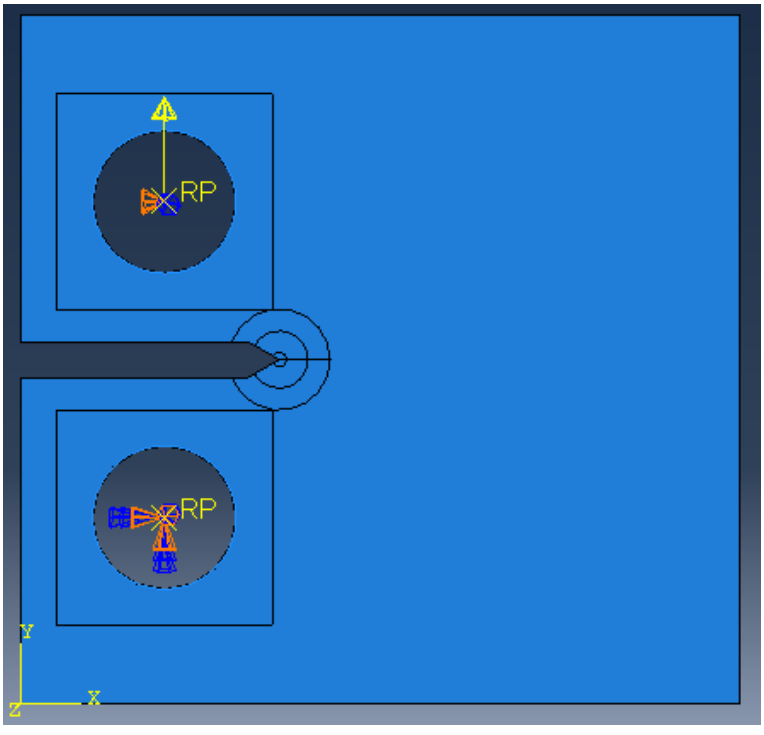

Figure 3.7 Loads and boundary conditions on assembled model.

3.1.5 Two-Dimensional Mesh

The mesh for this model consists of 8-node biquadratic plane-strain quadrilaterals with reduced integration (CPE8R) throughout the entire specimen. This element type was selected because of the ability to manipulate the midside node positioning for quadratic elements at the crack tip. Using the same element elsewhere in the model eliminates the opportunity for a mesh order compatibility error. The area inside the first partition circle is meshed using a sweep of quad-dominated elements. The area inside the second and third partition circles are meshed using a structured quadrilateral mesh method, and all other regions are meshed using a quadrilateral free mesh. The structured mesh attempts to create the most grid-like mesh possible. Free meshes use software-specific algorithms to mesh the volume by keeping elements as close to the approximate global size as possible, however, this can sometimes lead to poor aspect ratios. The mesh seeding on the circular partitions create a polar-plot type element pattern with each element at a sweep angle of 15 degrees. Additionally, 15 biased nodes connect the crack tip to the farthest circular partition. This bias places nodes closer together near the crack front and farther away from each other away from it. The squares around the circles are biased at a ratio of 1.5 towards the corner in contact with the crack zone focus mesh. This bias assures there is adequate mesh density for load transfer between the pinholes and crack front. The full mesh is shown in Fig. 3.8(a) and the mesh focus around the crack tip is shown in Fig. 3.8(b)

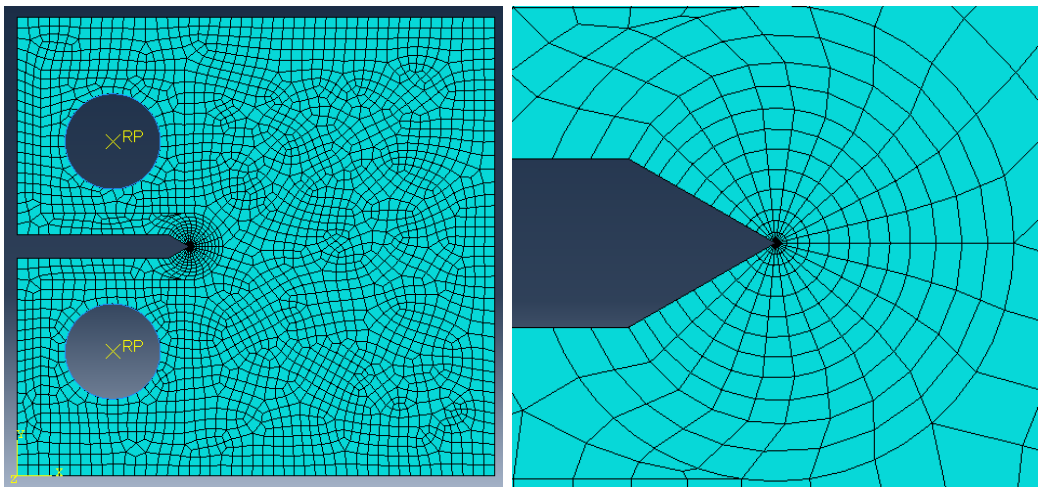

Figure 3.8 (a) Full meshed assembly. **(b)** Focus mesh around crack front.

Once the mesh was set and verified, the model was run to produce field outputs for stress, strain, displacement, and strain energy density and history outputs of the stress intensity values, K_I, K_{II}, K_{III} .

3.2 Two-Dimensional Linear Elastic Finite Element Model Results

This section summarizes key results from the two-dimensional model runs. The results discussed in this section are maximum principal stresses and stress tensor components, the displacement of the pins to verify boundary conditions, and the stress intensity factor at the crack tip.

3.2.1 Stress and Energy Results for the Two-Dimensional Linear Elastic Model

The contour plots shown below in Fig. 3.9 and Fig. 3.10 demonstrate the load transfer from the actuated top pin to the fixed bottom pin where the load is reacted. The stress clearly peaks at the sharp tip of the inlet where the crack front is located. Figure 3.9 shows the von Mises stress across the entire compact specimen and Fig. 3.10 shows the Y-directional stress in the area local to the crack front.

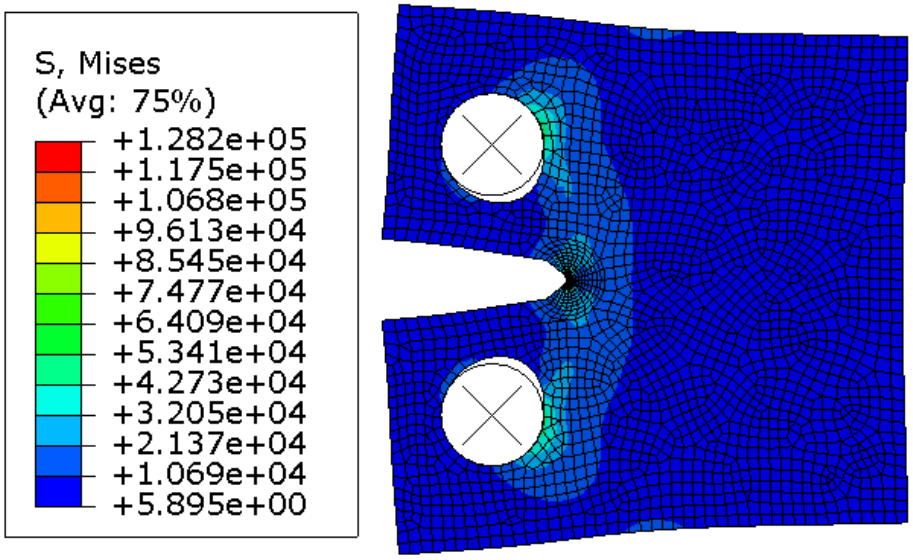

Figure 3.9 Full model von Mises stress contour plot.

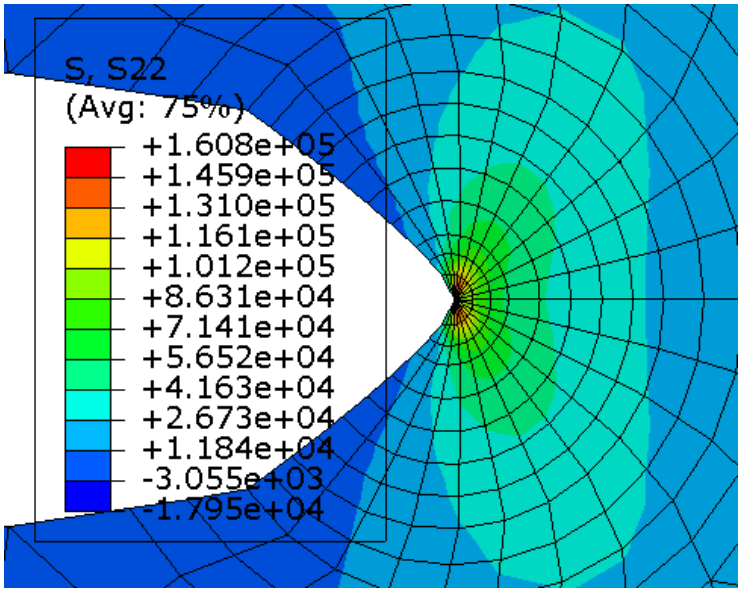

Figure 3.10 Y-direction stress contours local to crack front.

.

The maximum stress that occurred at the crack tip in the Y-direction was 161 ksi, which would have caused localized yielding at this location. The elastic strain energy density is shown in the contour plot in Fig. 3.11

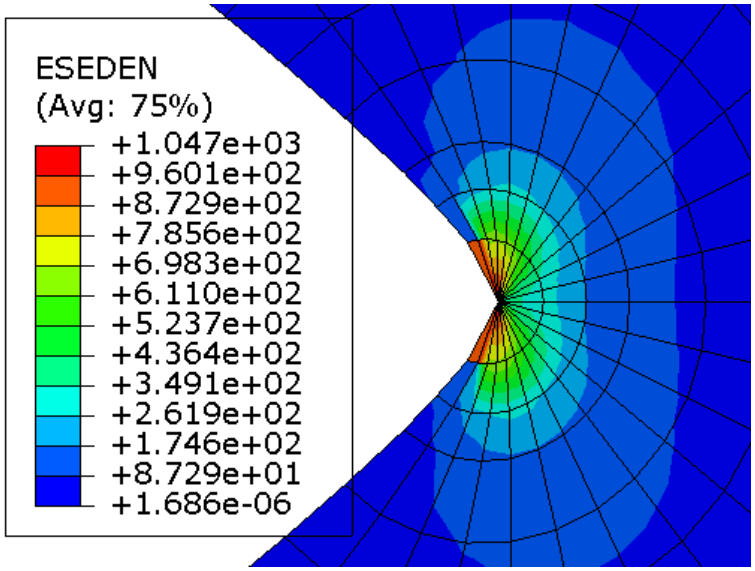

Figure 3.11 Elastic energy density contour plot.

Both the counter plots for stress and elastic strain energy density local to the crack tip show that the load is being appropriately distributed to the crack front and that the crack front opening behavior is occurring as expected in this model.

3.2.2 Displacement Results for the Two-Dimensional Linear Elastic Model

This model was loaded using a load-controlled approach, which means that the displacement response at the pins is a result of the model. The displacement contour plot for this model is shown in Fig. 3.12 below.

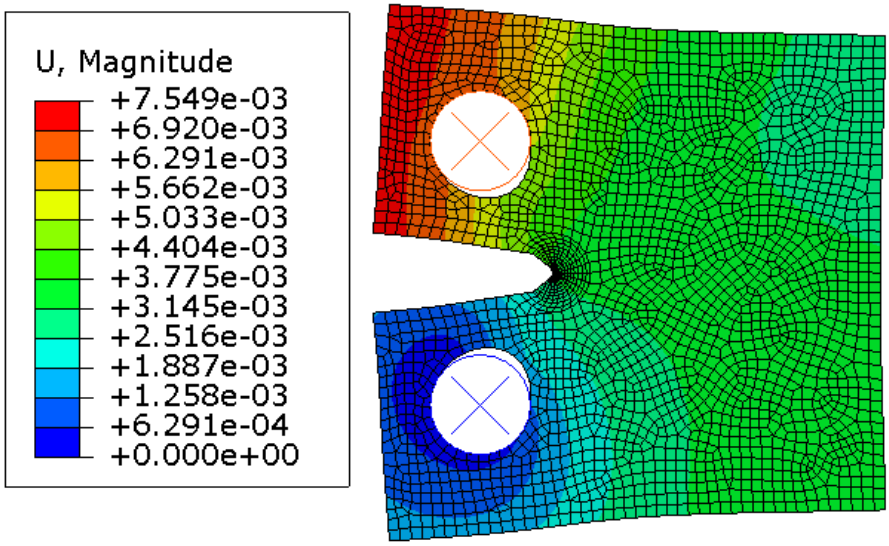

Figure 3.12 Displacement magnitude for two-dimensional model.

The displacement at the top pin for this model is 0.00649 inches and at the bottom pin there is no displacement. Neither pin has any displacement in the X-direction, which validates that the boundary conditions were appropriately executed in the model.

3.2.3 Stress Intensity Factor Results for the Two-Dimensional Linear Elastic Model

These results are consistent with the expected model behavior and the mesh converged. Therefore, the stress intensity factor can be examined from the history output file. When reading the contour integrals, the integral that occurs directly at the singularity should be ignored. The subsequent integrals, however, must agree to be considered an acceptable model. The second, third, fourth, and fifth contour integrals for this model were all within 0.1% with the consensus stress intensity factor, K, equaling 18.57 ksi$\sqrt{\text{in}}$. This is the K_I value; other K directional values are not reported because they were less than 1% of the K_I value. This stress intensity factor is less than the fracture toughness regardless of grain direction so according to Eqn. 2.8 fracture would not initiate for this loading and geometry.

The mesh convergence was determined based on the stress intensity factor at the crack front as shown in Eqn. 3.1 shown below.

$$\%_{Difference} = \left[\frac{\{K_{I\,Mesh2} - K_{I\,Mesh1}\}}{K_{I\,Mesh1}}\right] * 100 \quad (3.1)$$

For this model the $\%_{Difference}$ = 0.3% for the mesh used as the final model mesh.

3.3 Analytical Validation of Two-Dimensional Finite Element Model Results

The results obtained from the finite element model were verified using analytical methods outlined in Dowling's 4th Edition [3]. The nomenclature used for the analytical methods corresponds to the dimensions in Fig. 3.13.

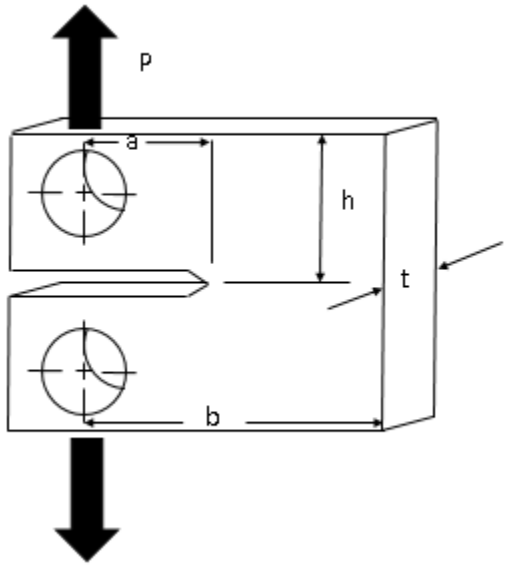

Figure 3.13 Key dimensions for closed-form solution.

For our model, the dimensions referenced in Fig. 3.1 are shown in Table 3.6.

Table 3.6 Reference Dimensions for Fig. 3.1

Parameter	Length (in)
A	0.4
B	2
H	1.2
T	0.125

Before any of the analytical equations are used, $\frac{h}{b}$ must be verified to be equal to 0.6. For this analysis $\frac{h}{b} = \frac{1.2}{2} = 0.6$. The rest of the analytical equations are as follow in Eqn. 3.2, Eqn. 3.3, and Eqn. 3.4.

$$\alpha = \frac{a}{b} \tag{3.2}$$

$$F_P = \frac{2+\alpha}{(1-\alpha)^{\frac{3}{2}}}(0.886 + 4.64\alpha - 13.32\alpha^2 + 14.72\alpha^3 - 5.6\alpha^4)\ for\ \alpha \geq 0.2 \tag{3.3}$$

$$K = F_P\left(\frac{P}{t\sqrt{b}}\right) \tag{3.4}$$

For this study, the following values were calculated from the equations listed above: α=0.2, F_P=4.21, and K= 23.83 ksi$\sqrt{\text{in}}$. The P value is the 1,000 lbf concentrated force applied to the actuated pin in the model. This stress intensity value is not consistent with the stress intensity value obtained from the finite element model. This is because the finite element model accounts

for tangential friction on the pins but the closed-form analytical model does not account for the non-vertical component of the load due to friction. This disparity causes the model to account for horizontal loading and energy lost to friction that the closed-form solution does not include. When the tangential friction interaction control was replaced with a frictionless parameter the stress intensity factor for the model increased to 23.35 $ksi\sqrt{in}$ with contour integrals two through five all within 0.2% of each other. This stress intensity value has an error of 6% from the closed-form analytical value. This value is acceptable because the closed-form value relies on the plane strain assumption. The plane-strain closed-form estimate was closer than the plane stress estimate; however, the true behavior is not encompassed by either estimate. The elastic energy density at the crack tip increased by 44.7% after the tangential interaction friction coefficient was changed to frictionless.

The relatively low percent error supports the goal that the techniques used for meshing, applying loads and boundary conditions, and constructing the geometry are valid for this model. The next step in the research will explore a three-dimensional linear elastic fracture model for this same compact specimen geometry.

4. Three-Dimensional Linear Elastic Model

The second phase of this research develops and explores a three-dimensional linear elastic model in an effort to better represent the specimen physics. The main phenomenom neglected by the two-dimensional linear elastic model from Chapter 2 is that there is inhomogeneous stress through the thickness of the specimen. The variation of the mechanics occurring through the specimen thickness are not accounted for in the two-dimensional model. The three-dimensional model also allows for the deformation along the crack front to be visualized. This visualization of the deformed shape provides a qualitative method for verification that the model is accurately replicating the behavior of the compact specimen test from ASTM E399 that occurs in a load frame.

In the subsequent sections of this chapter, the modeling technique for this three-dimensional model will be discussed and the results for the three-dimensional linear elastic model will be explored. The results from the model will be verified using the closed-form frictionless analytical solution [3] and by comparison to the two-dimensional linear elastic model from Chap. 3.

4.1 Three-Dimensional Linear Elastic Finite Element Model Development

The development of the three-dimensional linear elastic fracture mechanics model iterates on the techniques from the two-dimensional linear elastic fracture mechanics model. The following section discusses the techniques to model the compact specimen fracture in three dimensions.

4.1.1 Three-Dimensional Part, Partitioning, and Material

The model was developed using the dimensional convention from Fig. 3.1 and is identical to the geometry used for the two-dimensional model except for the method that the thickness is explicitly represented by the geometry. The thickness is generated by extruding the sketch geometry to the thickness of t = 0.125 in. The partitioning scheme for this geometry, however, is different from the scheme used in the two-dimensional model study. Figure 4.1(a) and Fig. 4.1(b) below show the partitioning scheme utilized in this model.

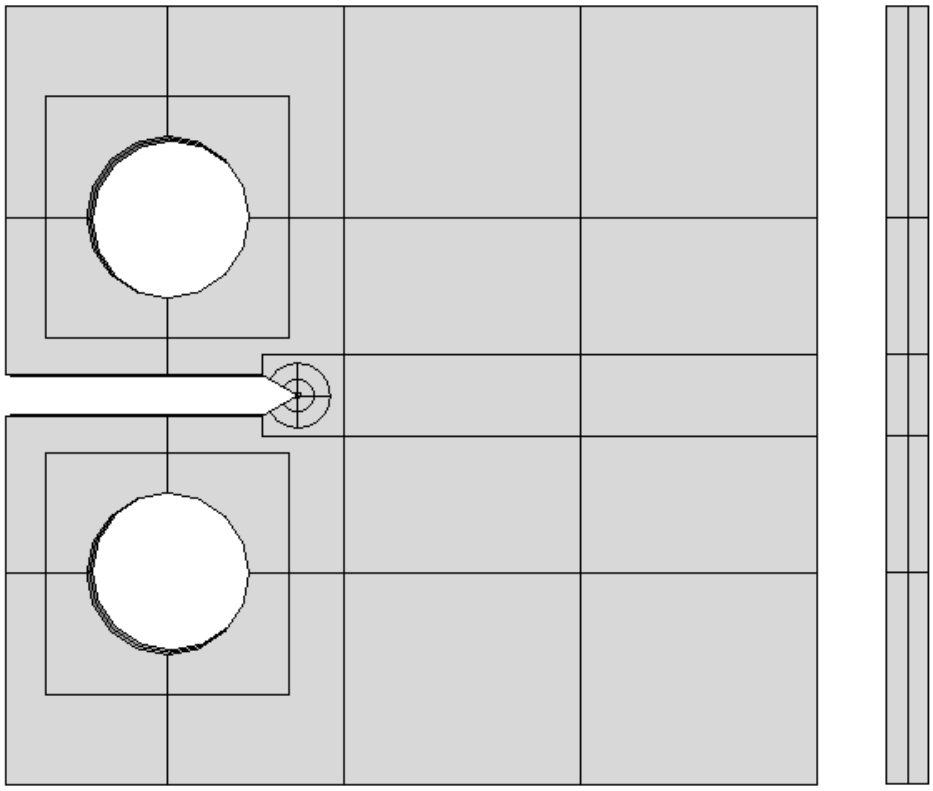

Figure 4.1(a) XY partitioning scheme. **(b)** YZ partitioning scheme.

The partitioning scheme for this geometry consists of two hole focus regions and one crack tip focus region. The hole focus regions are 0.75 inch squares centered at the center of the hole. These focus meshes allow for increased mesh density around the holes so that the contact

pressure can appropriately be distributed from the holes. These focus meshes are partitioned in quarters so that the meshes for the four corners can be independently adjusted to allow for higher mesh density at the corners that are transferring load through the crack front to the other pin. The lines that create the hole focus mesh quartering are extended to the edge of the specimen. This partitioning scheme allows for more control over the transition from the focus mesh to the global mesh on the rest of the geometry. The crack front focus mesh consists of three concentric circles divided every 90 degrees by line partitions. This common crack tip modeling partition scheme allows there to be a polar-plot type pattern, which is highly conducive to consistent contour integral values. The partition radii for this model are listed in Table 4.1.

Table 4.1 Radial Dimensions for Focus Partitions Local to Crack Tip

Partition	Radius (in)
R0	0.01
R1	0.05
R2	0.1

A rectangular partition encloses the circular partitions and intersects with the origin of the two surfaces that form the crack tip. This partition is to facilitate high quality elements in the load transfer path between the holes and the crack tip by transitioning the crack-tip focus mesh to the global mesh. The partitions that make up the transition rectangle are extended to the edges of the specimen to provide additional opportunities to refine the mesh. The final partition, shown in Fig. 4.1(b), is a partition down the center of the thickness of the specimen. This partition functions to ensure that there is a node set for contour integrals to be taken exactly at the center of the specimen. As discussed earlier, the stress intensity changes through the thickness of the specimen with the highest stress intensity value at the center. Similar to the two-dimensional model, an *Analytical Rigid* part is created to simulate the machine pins used to load the specimen. These pins were constructed identically to the pins in the two-dimensional model; however, these pins were extruded to a depth that equaled the extruded thickness of the three-dimensional specimen.

The properties for this model are identical to the properties for the two-dimensional model with the model specimen material being Aluminum 7075-T651. This material's properties are defined in Table 3.3. This material is applied to the entire compact specimen model and is considered homogeneous, isotropic and perfectly elastic in this model.

4.1.2 Three-Dimensional Assembly and Interaction

The compact specimen is assembled with the machine *Analytical Rigid* pins. A coincident constraint is used to position each pin in the XY plane and a translational constraint is applied to position it in the Z-direction. Each pin is assigned a contact interaction with the inside of the hole on the compact specimen model to which it corresponds. The rigid analytical pin is the master surface and the compact specimen hole is the slave surface. These contact interactions only allow for overclosure adjustment. These properties, as shown in the Abaqus dialog box, are shown in Fig. 3.3. The contact property for these interactions is a hard contact in the normal direction with penalty enforcement, linear behavior, a stiffness scale factor of 1 and separation allowed after contact. The friction coefficient is set to 0.61 in the tangential direction, which is the coefficient of friction between tool steel and aluminum [12]. The interaction properties used in this model are shown in the Abaqus dialog window in Fig. 3.4. The tangential property is set to frictionless for validation so the model is consistent with the assumptions in the closed-form solution. The tangential friction coefficient is the only parameter that is altered between the model designed to replicate the physical experiment and the model designed to be used for model verification with the closed-form solution.

The crack is also implemented as an interaction. The crack front of this model is the edge formed by the intersection of the two angled surfaces that make up the sharp crack tip at the end of the inlet. The q-vector direction cosine, which controls the crack growth direction, is (1,0,0). This crack has a midside node moved to the quarter point and degenerate crack tip nodes. The degenerate nodes reduce to a single node on the collapsed element side as is required when doing a linear elastic fracture model [1]. Figure 3.6 earlier stated the input to the Abaqus dialog box to obtain these fracture singularity properties.

Figure 4.2 shows the model with all interaction properties displayed, the crack front is represented by the red line with a green “X” marking each end and the yellow squares represent the contact surfaces.

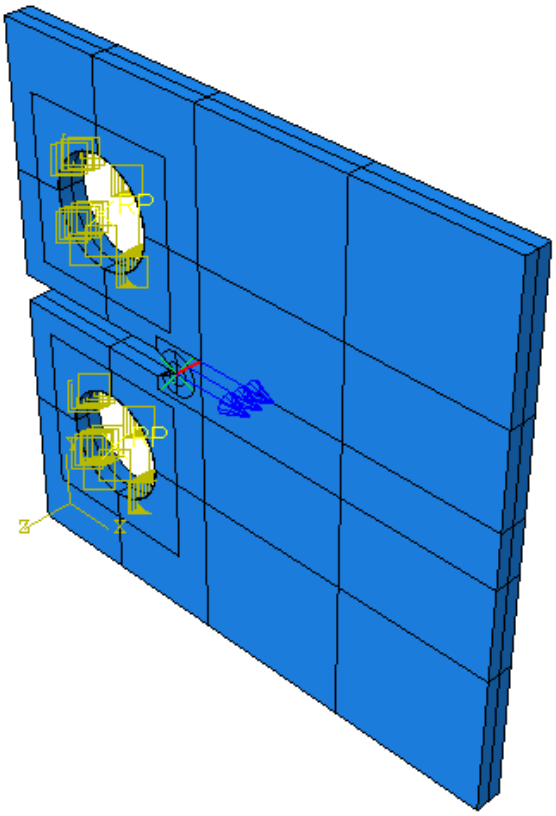

Figure 4.2 Three-dimensional compact specimen interactions.

4.1.3 Three-Dimensional Loads and Boundary Conditions

The boundary conditions on this model are applied to the machine pins and then through contact imposed on the compact test specimen. The bottom pin is fixed, therefore, no translations or rotations in any direction are permitted for the bottom pin. The top pin has a boundary condition that only allows translation in the Y-direction, the direction in which it is being loaded, and no other translations or rotations are permitted. It is important to note that the contact

interaction permits the compact specimen material to slide around the pin; however, the pin itself is not allowed to rotate. These boundary conditions are shown in Table 4.2.

Table 4.2 Three-Dimensional Linear Elastic Boundary Conditions Table

Location	**Boundary Condition**
Bottom Pin	U1=U2=U3=UR1=UR2=UR3=0.0
Top Pin	U1= U3=UR1=UR2=UR3=0.0

The top pin is loaded in the positive Y-direction with a concentrated force on the reference point at the center of the pin with a magnitude of 2,000 lbf. All boundary conditions are applied during the initial step while the load is not applied until the subsequent loading step. The load case is shown below in Table 4.3.

Table 4.3 Three-Dimensional Linear Elastic Loads Table

Location	**Load**
Top Pin	CF2=2000.0 lbf

The model with loads and boundary conditions displayed is shown in Fig. 4.3.

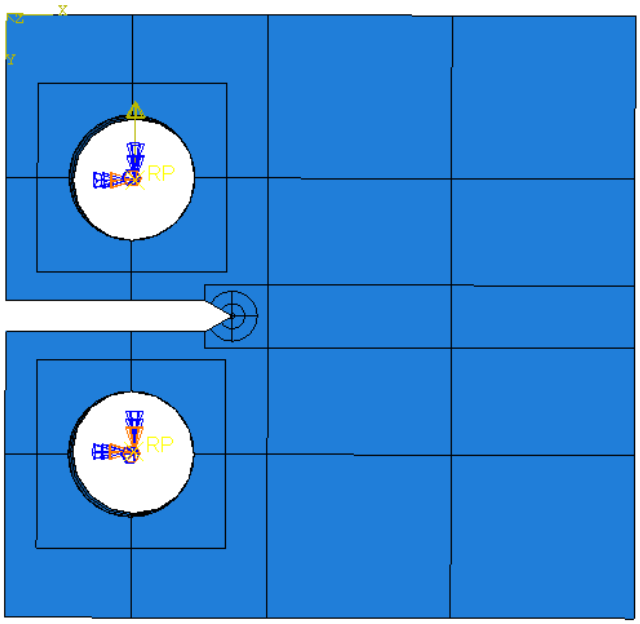

Figure 4.3 Three-dimensional compact specimen with loads and boundary conditions shown.

4.1.4 Three-Dimensional Mesh

The meshing strategy for this model was to ensure a constant high mesh density path from the contact area of the hole to the crack tip so that the load transfer was properly modeled. The crack-focus mesh area has 20-node quadratic brick, hybrid, linear pressure, reduced integration elements (C3D20RH) which have exactly a 15-degree sweep angle and vary in size based on proximity to the crack front. There are 13 concentric rings of elements that comprise this focus mesh. These elements started as hexahedral elements (brick elements) but once the edge of the face is collapsed and nodes combined, they become wedge shaped. The remainder of the cells within the load transfer region, including the focus meshes around the pinholes, are 20-node quadratic brick reduced integration elements (C3D20R) that are biased towards the load path. This means that there is a smaller distance between mesh seeds closer to the crack front than farther from the crack front. The remainder of the elements are globally seeded to a size of 0.125 inches are 8-node linear brick, reduced integration, hourglass control (C3D8R). This model takes advantage of the partitioning to use higher order elements only within the load transfer path and uses linear elements in the remainder of the cells. Finally, the through-thickness

direction is seeded with 20 elements for the entire model. This through-thickness direction mesh density allows the crack front behavior to be observed in the middle of the specimen where it is without free surface effects. This through-thickness seeding creates acceptable aspect ratios for the elements nearest the crack front. The element type regions are shown in Fig. 4.4 and the final part mesh is shown in Fig. 4.5

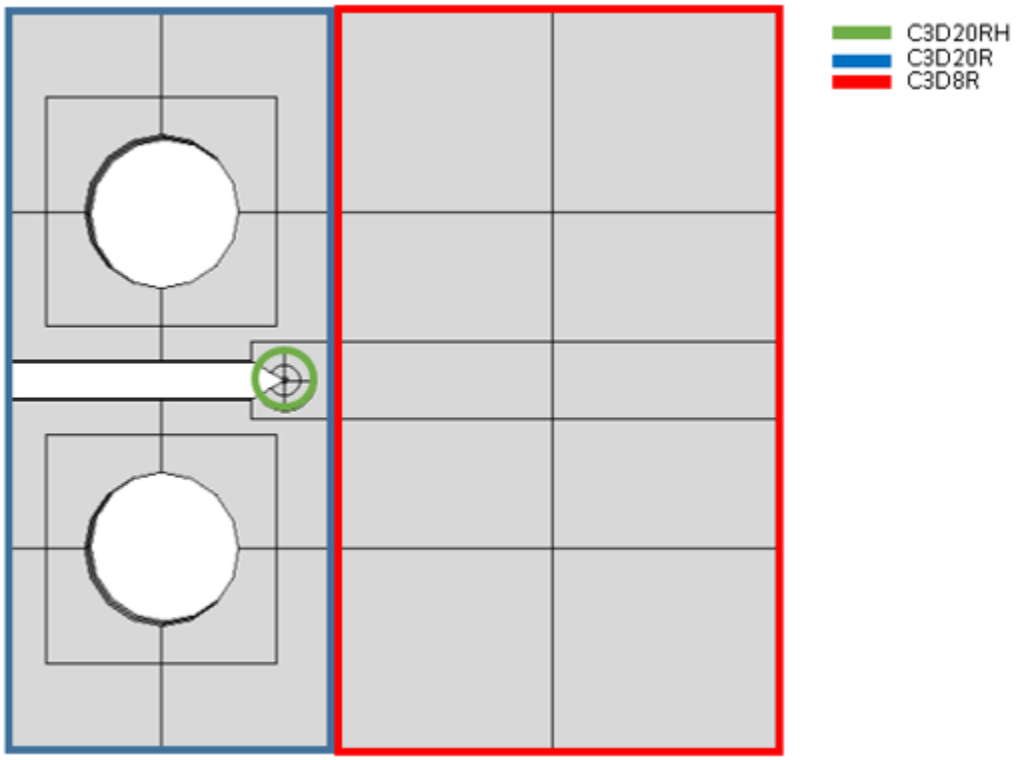

Figure 4.4 Three-dimensional model colored by element type.

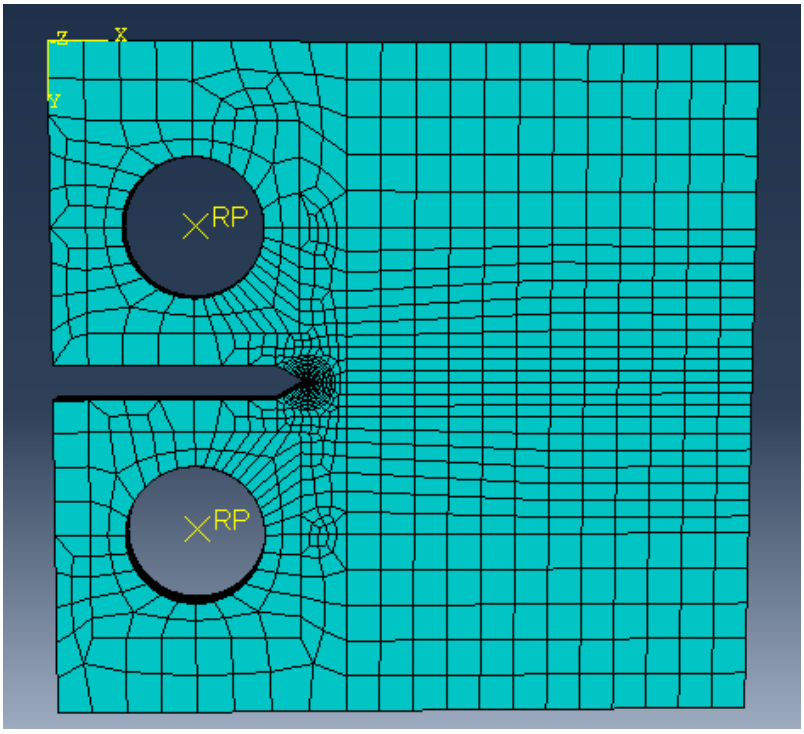

Figure 4.5 Meshed three-dimensional model.

4.2 Three-Dimensional Linear Elastic Finite Element Model Results

The three-dimensional linear elastic model was run as discussed in Chap. 4.1 and the results for stress, strain, strain energy density, displacement, and stress intensity factor were collected.

4.2.1 Three-Dimensional Stress and Energy Results

Figure 4.6 shows that the Y-Direction stress intensity around the crack tip has the expected shape, which reaches from the tip towards the two pinholes that supply and react the load. The Y-directional stress contour is shown in Fig. 4.6 and the von Mises stress contour for the entire specimen is shown in Fig. 4.7. The contour plot in Fig. 4.7 shows the load transfer through the specimen.

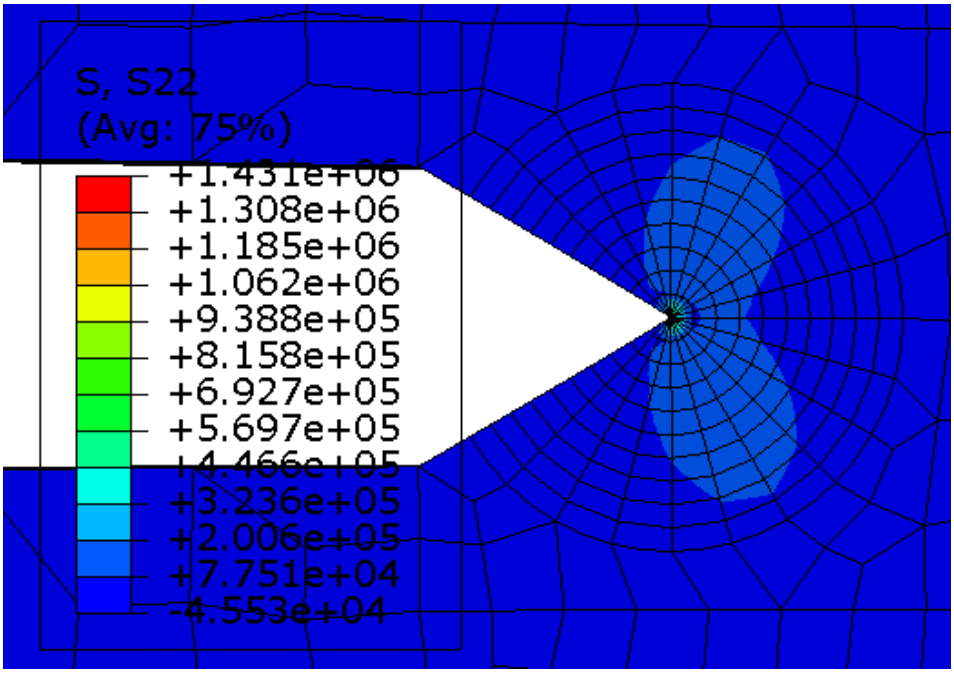

Figure 4.6 Y-direction stress zone around crack tip

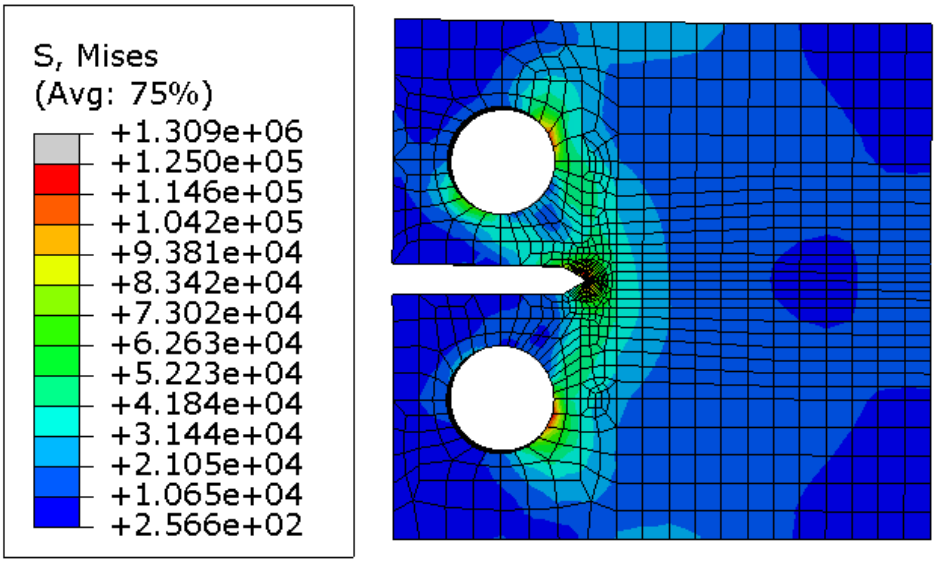

Figure 4.7 von Mises stress contour for full compact specimen.

The maximum stress is 315 ksi and occurs at the crack tip in the center of the thickness of the model. Larger stress values, as high as 1,430 ksi, are displayed in the contour plot. This is

not an accurate stress value since plasticity is not accounted for in this model. The area around the crack tip enters the plastic region; however, the stress is still determined according to Young's Modulus. Figure 4.7 verifies the expected load distribution path. Figure 4.8 also verifies the load distribution via elastic strain energy density contours.

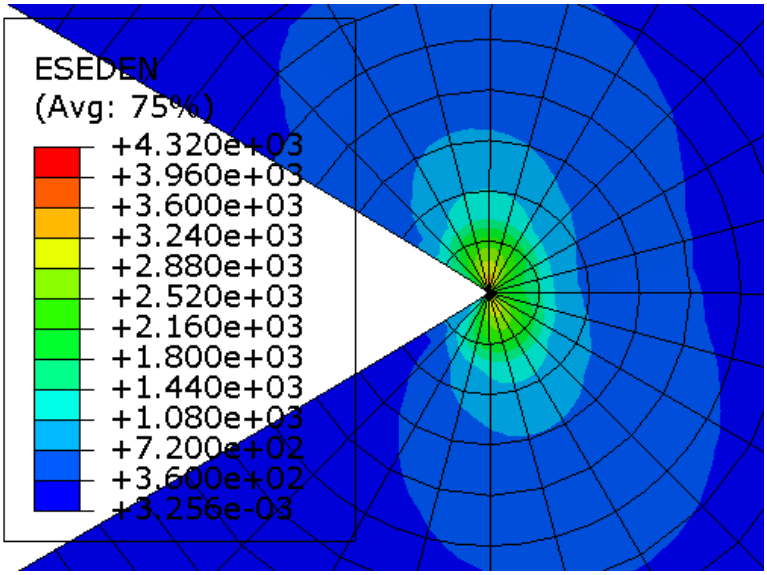

Figure 4.8 Strain energy density contour plot.

The area around the crack tip has the highest strain energy density since this area experiences the most strain.

The through-thickness stress contour plot in the local region around the crack tip demonstrates the capability of the three-dimensional model to capture the edge effect behavior. This contour plot is shown in Fig. 4.9.

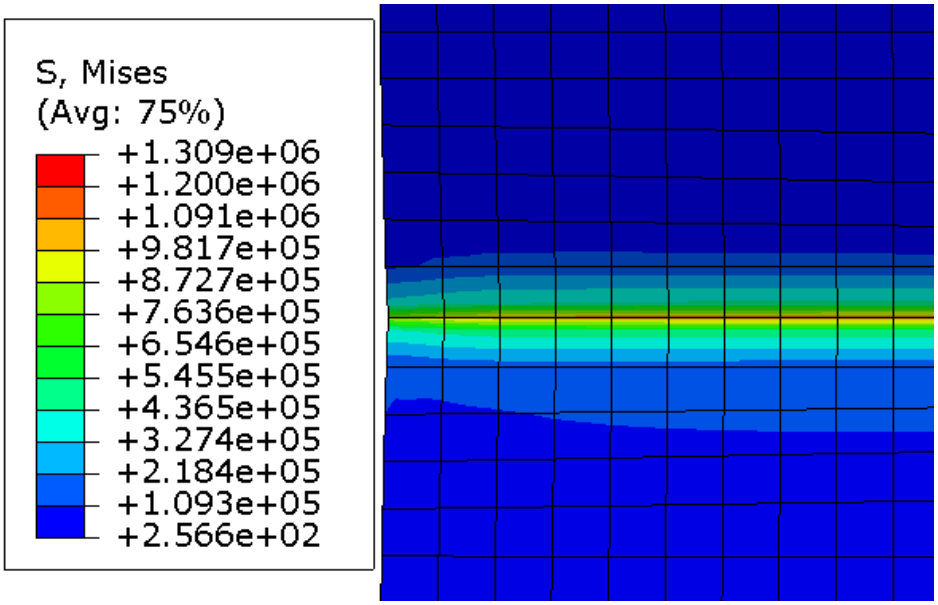

Figure 4.9 Stress at crack tip YZ contour plot for half the thickness.

4.2.2 Three-Dimensional Displacement Results

The three-dimensional linear elastic fracture mechanics model was loaded using a load-controlled strategy. The displacement results are investigated to verify that the model behaves as expected and that boundary conditions are maintained. Figure 4.10 shows the displacement results for the three-dimensional linear elastic model.

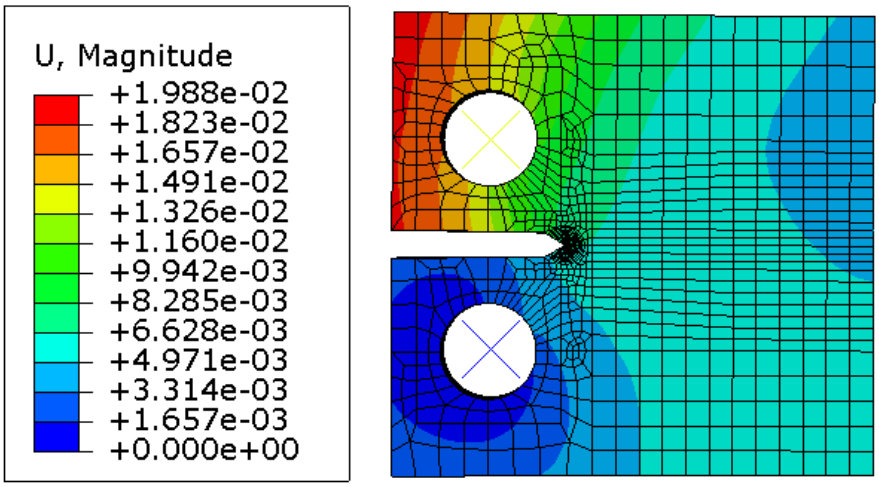

Figure 4.10 Displacement magnitude for full model.

The top pin displaced 0.0148 inches solely in the Y-direction and the bottom pin remained fixed. The top pin displacement is about twice as much as the two-dimensional case where the load was half as much. This verifies that the boundary conditions were properly applied to replicate the load frame test.

4.2.3 Three-Dimensional Stress Intensity Factor Results

The stress intensity factor for the case where friction was accounted for to simulate the experimental load frame case was 44.18 ksi$\sqrt{\text{in}}$ with contour integrals two, three, four, and five all within 0.5% of each other. The frictionless case that will be used for model verification against the closed-form solution had a stress intensity factor of 47.39 ksi$\sqrt{\text{in}}$ with contour integrals two, three, four, and five all within 1.7% of each other. The K_I values were over two orders of magnitude more significant than both K_{II} and K_{III} for both friction properties.

The three-dimensional linear elastic model underwent multiple refinement iterations to converge the mesh density and to verify that the model behavior was correctly replicating the part behavior when tested in the load frame. The $\%_{\text{Difference}}$ convergence criteria for this model, calculated using Eqn. 3.1, was 0.85% based off the stress intensity factor, K_I.

4.3 Validation of Three-Dimensional Finite Element Model Results

The same verification method was used for the two-dimensional and three-dimensional model. The closed-form analytical model is compared to the model result from the case of a frictionless run. Using Eqns. 3.2, 3.3, and 3.4 from Chap. 3.3 the stress intensity factor from the closed-form analytical approach is 47.66 ksi$\sqrt{\text{in}}$. The only parameters that changed between this calculation and the calculation in Section 2.3 is the load was doubled from 1,000 lbf to 2,000 lbf in the three-dimensional model. The frictionless model that best represents the boundary conditions used in the closed-form approach calculated a stress intensity factor of 47.39 ksi$\sqrt{\text{in}}$. which is 0.57% off the closed-form solution. The stress intensity results for Chap. 3 and Chap. 4 are summarized in Table 4.4. The load normalized stress intensity factor for the compact tensile specimen geometry can be calculated according to Eqn. 4.1.

$$\frac{K_I}{F_P} = \left(\frac{P}{t\sqrt{b}}\right) \tag{4.1}$$

The K_I value should be linear with respect to the load, P, so there should be no difference between the two and three-dimensional normalized K_I values. The normalized K_I values for the two-dimensional and three-dimensional linear elastic fracture mechanics models have a percent difference of 0.43% for the frictionless model results.

Table 4.4 Summary of Stress Intensity Factors from Chap. 3 and Chap. 4

Model	**K_I with Friction** $ksi\sqrt{in}.$	**K_I without Friction** $ksi\sqrt{in}.$	**K_I from Analytical** $ksi\sqrt{in}.$	**% Error without Friction**	**Normalized K_I without Friction** $\frac{ksi\sqrt{in}}{lbf}$
Two-Dimensional	18.57	23.35	23.83	6%	0.02335
Three-Dimensional	44.18	47.39	47.66	0.57%	0.023695

The three-dimensional fracture model stress intensity factors exceed the fracture toughness for Aluminum 7075-T651 regardless of grain direction. This means that according the Eqn. 2.8 fracture would initiate. The three-dimensional linear elastic model represents the closed-form solution for stress intensity factor so it will be the baseline from which the plastic model is built. This model qualitatively and quantitatively is shown to represent the elastic fracture conditions well. The model will continue to be developed in Chap. 5 as plasticity is included. According to Eqns. 2.5, 2.6, and 2.7, the J-integral for the three-dimensional linear elastic fracture model with pin friction was 127 [psi-in].

5. Three-Dimensional Plasticity Model

The final step in this research is the generation of a fracture model that has residual stress states at the crack tip before the fracture initiation. This model does not have a closed-form solution or any experimental data that could be used to verify it, like the linear elastic models from Chapter 3 and 4 did. As such, the methods used in the model have to be properly verified systematically. First, the previous two models serve to establish the meshing strategy and scheme with regards to partitioning, element sizing, and element spacing. Second, dog bone supplemental models are run to verify that the plastic material properties are behaving in a way that is consistent with the stress-strain curve for the given material. Another dog bone supplemental test is conducted to verify that the submodeling methods are valid. These dog bone supplemental tests proved to be instrumental in understanding how Abaqus replicates physical phenomena in the simulation space.

In this chapter, the major steps in developing the three-dimensional plasticity model will be discussed. The major steps are as follows: developing a quasi-static model to generate a plastic zone in the compact specimen, verifying the results of the quasi-static model using closed-form plastic zone size estimates, developing a fracture submodel from the quasi-static model, and exploring the results from the analysis of fracture submodel.

5.1 Quasi-Static Plastic Model Development

A key difference that separates the model developed for the quasi-static global model is that this model is developed to obtain the far-field quasi-static displacement field instead of fracture properties. The previous models needed to accurately model the load transfer from the pins to the crack front whereas this model is solely focused on development of the plastic zone around the crack tip.

5.1.1 Quasi-Static Plastic Part and Partition

The part geometry that is used in this model is identical to the geometry used in the three-dimensional model. The distance from the back of the compact specimen to the center of the load pins, *w*, is still 2 inches and the thickness of the part is still 0.125 inches. The complete dimensions of the compact specimen are provided in Table 3.1. The partitioning scheme for this model has been changed so that the circular partitions from the previous two models are removed. This scheme was used because the main goal of this model is accurate quasi-static plastic deformation on a macroscopic part level. The goal of the two and three-dimensional linear elastic model was to accurately capture the behavior of the crack tip at the singularity. With this in mind, the final partitioning strategy involved a rectangular partition around the area local to the crack tip where the plastic zone will develop. This partition shares an edge with the square partition around each of the pinholes. These partitions ensure that the pinholes are meshed adequately to distribute the contact load into the compact specimen. The partitioning scheme is shown below in Fig. 5.1.

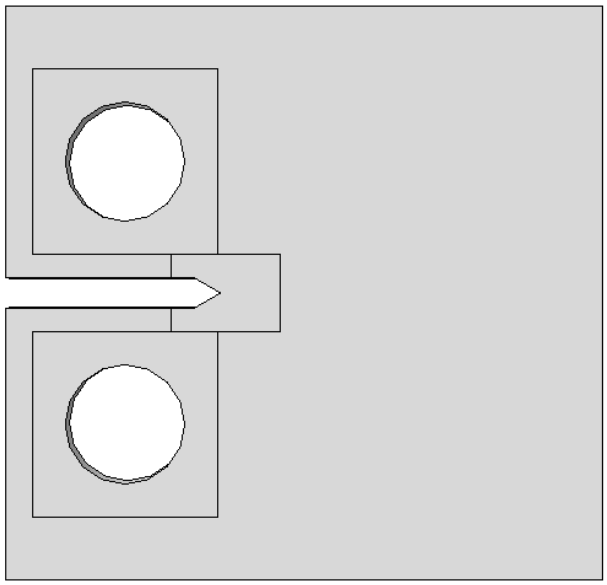

Figure 5.1 Partitioning scheme for plastic quasi-static model.

Similar to the linear elastic models, rigid analytical pins are created to simulate the interaction between the load frame and the compact specimen. These *Analytical Rigid* pins are given a central reference point and are not meshed components of the model, since the deformation of the steel pins when in contact with aluminum is negligible.

5.1.2 Quasi-Static Plastic Section and Material

One section property is specified for this model and is homogeneously applied to the entire compact specimen part. The section utilizes a material property that represents Aluminum 7075-T651 in both the elastic and plastic regions. Both the elastic and plastic properties were developed from nominal test data provided in Table E12.1 of Dowling's 4th edition [3]. The material is isotropic with elastic properties defined by a Young's Modulus of 10.26 x 10^6 psi and a Poisson's ratio 0.33. These values are within 0.5% of the values used in the linear elastic models in the previous chapters shown in Table 3.3.

The plastic material response region is defined by isotropic hardening and the following tabular data, shown in Table 5.1, extracted from the data in Dowling [3].

Table 5.1 Nominal Plastic Tabular Aluminum 7075-T651 Data from Dowling Table E12.1

Yield Stress (psi)	**Plastic Strain (-)**	**Yield Stress (psi)**	**Plastic Strain (-)**
64391.07	0	71789.46	0.021002
65197.48	0.000645	71922.89	0.021989
66066.26	0.00156	72053.43	0.022977
66753.74	0.002493	72176.71	0.023964
67323.74	0.003438	72297.09	0.024953
67809.62	0.00439	72413.12	0.025941
68233.13	0.005349	72526.25	0.02693
68607.33	0.006312	72635.03	0.02792
68945.26	0.00728	72739.46	0.02891
69251.29	0.00825	72842.43	0.0299
69531.22	0.009222	72941.06	0.03089
69789.38	0.010197	73038.24	0.031881
70028.7	0.011174	73131.06	0.032871
70253.51	0.012152	73222.43	0.033863
70462.36	0.013132	73312.36	0.034854
70659.61	0.014112	73397.93	0.035845
70846.71	0.015094	73483.5	0.036837
71022.21	0.016077	73566.17	0.037829
71190.45	0.017061	73645.95	0.038821
71349.99	0.018045	73725.72	0.039814
71503.73	0.01903	73802.59	0.0428
71648.77	0.020016		

The Ramberg-Osgood constants for this material data in the form of Eqn. A.3 are:$H = 84{,}920$ psi, $E = 10{,}260{,}000$ psi, and $n = 0.0445$. *Deformation Plasticity* definitions, such as Ramberg-Osgood, cannot be used for this particular model because Abaqus's *Deformation Plasticity* material definitions are not valid for elastic-plastic unloading. *Deformation Plasticity* Abaqus material definitions are designed to be used only for non-linear elastic monotonic loading. The material response of the Abaqus deformation plasticity model retraces the same curve it loaded on during unloading, similar to a nonlinear elastic response, instead of unloading elastically first then plastically if needed.

5.1.3 Quasi-Static Plastic Model Assembly and Interaction

The model is assembled by moving the pins into position in the XY plane using a coincident constraint with the center point of the pinholes and the reference point of the pin, then positioning in the Z-direction by translating the edge of the pin to the edge of the pinhole. The pins are used as the master surfaces for the contact interaction with the compact specimen and the slave surface is the inside of the compact specimen holes. The Abaqus dialog window assigning the properties that define this contact behavior is shown in Fig. 3.3. The contact property in the normal direction is specified as hard contact with linear behavior, penalty enforcement, and separation allowed after contact. In the tangential direction, the contact property is an isotropic penalty function with a friction coefficient of 0.61, the coefficient of friction between tool steel and aluminum [12]. The Abaqus dialog window for the interaction property definition is shown in Fig. 3.4. This model does not have any fracture singularity specified because this model is solely to determine the quasi-static displacement field and generate the plastic zone.

5.1.4 Quasi-Static Plastic Model Boundary Conditions

The load application for the quasi-static model changed from load-controlled to a displacement-controlled approach using a prescribed displacement. This change was made because prescribing the field variable is more stable. The load step in this model must permit non-linear geometry since the plastic zone creates displacements that are considered large displacements. This model is initialized with the bottom pin fixed to not permit any rotations or translations in any direction and the top pin is only free to translate in the Y-direction and no other rotations or translations are permitted as outlined in Table 4.2. These boundary conditions are propagated into the loading step. In the loading step, the model is loaded using a boundary condition that applies a prescribed displacement to the top pin in the Y-direction of magnitude 0.015 inches. This prescribed displacement has an amplitude acting on it, shown below in Table 5.2 and in Fig. 5.2.

Table 5.2 Top Pin Forced Displacement Loading Amplitude Tabular

Step Time (%)	Amplitude (-)
0	0
0.32	1
0.66	0
1	1

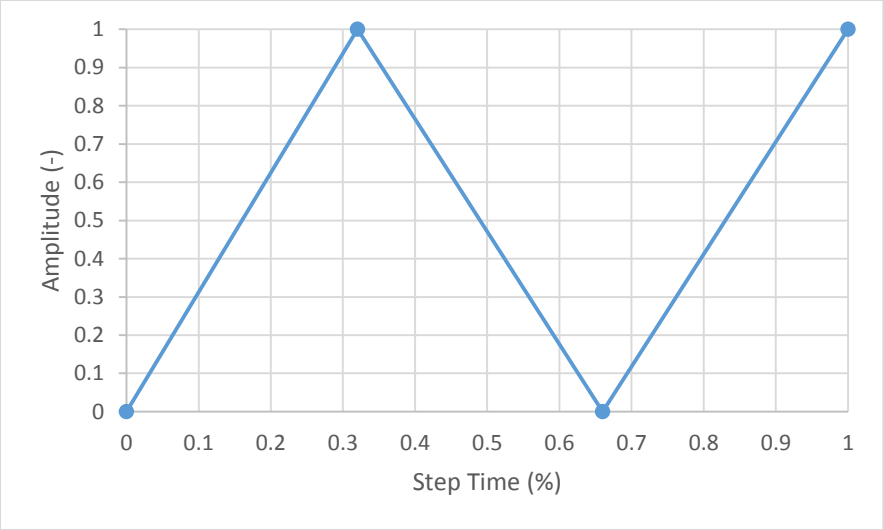

Figure 5.2 Top pin forced displacement loading amplitude plotted.

This amplitude demonstrates a Load-Unload-Reload sequence that is used in this fracture submodel. The first step applies a plastic strain to the part, the second step unloads the part, and finally the third step reloads the part and calculates stress intensity values in the plastic zone. The step times are nominally a third of the step duration, however, they are adjusted to run at a fixed increment of 0.02 (2% of load) per iteration. All three loading phases are incorporated into one model step using this amplitude function. Figure 5.3 shows the boundary conditions applied to the model during the loading step.

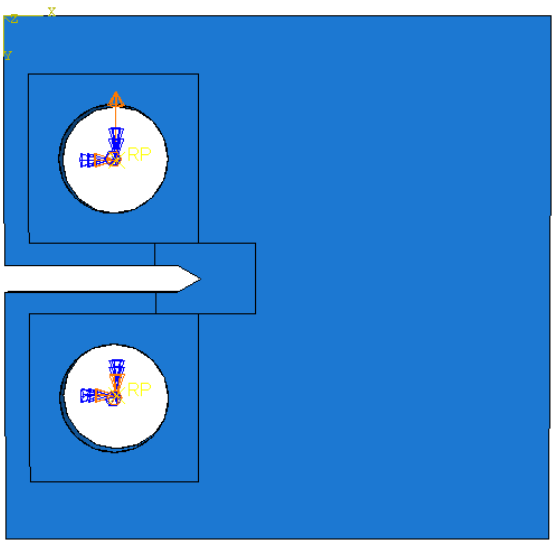

Figure 5.3 Boundary conditions for quasi-static plasticity model.

5.1.5 Quasi-Static Plastic Model Mesh

The main objective of the mesh in this model is to generate an accurate plastic zone around the region where the crack tip is located. To accomplish this, very fine mesh seeding is applied to the partition around the crack tip region. The mesh seeding ensures that the mesh inside and locally outside the partition will be dense. The mesh is brought to better focus around the pinholes. In the quasi-static model, however, this mesh quickly converged. The entire compact specimen is meshed using a sweep mesh of hexahedral (brick) elements, which provides the high mesh density in the partition targeted areas. Eight node linear brick, reduced integration, hourglass control elements (C3D8R) are used throughout the model since there is no singularity behavior that must be captured. The main objective of the model is to obtain a far-field displacement profile to use in the submodel. Therefore, the additional accuracy of the quadratic elements do not outweigh the additional computational expense. The mesh used in the quasi-static plastic run is shown below in Fig. 5.4

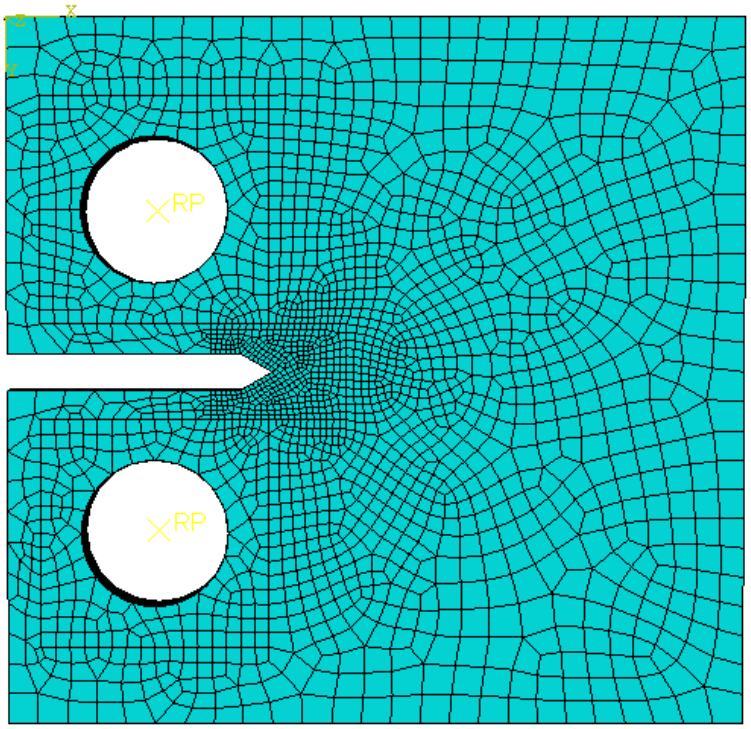

Figure 5.4 Mesh for quasi-static plastic model.

5.2 Quasi-Static Plastic Model Results and Verification

5.2.1 Quasi-Static Plastic Model Far-Field Stress

The model run generated a von Mises stress contour for the entire part. This single run replicated the Load-Unload-Reload behavior of the compact specimen. In Fig. 5.5, Fig. 5.6, and Fig. 5.7 the stress contours are shown at the three different steps in this load cycle.

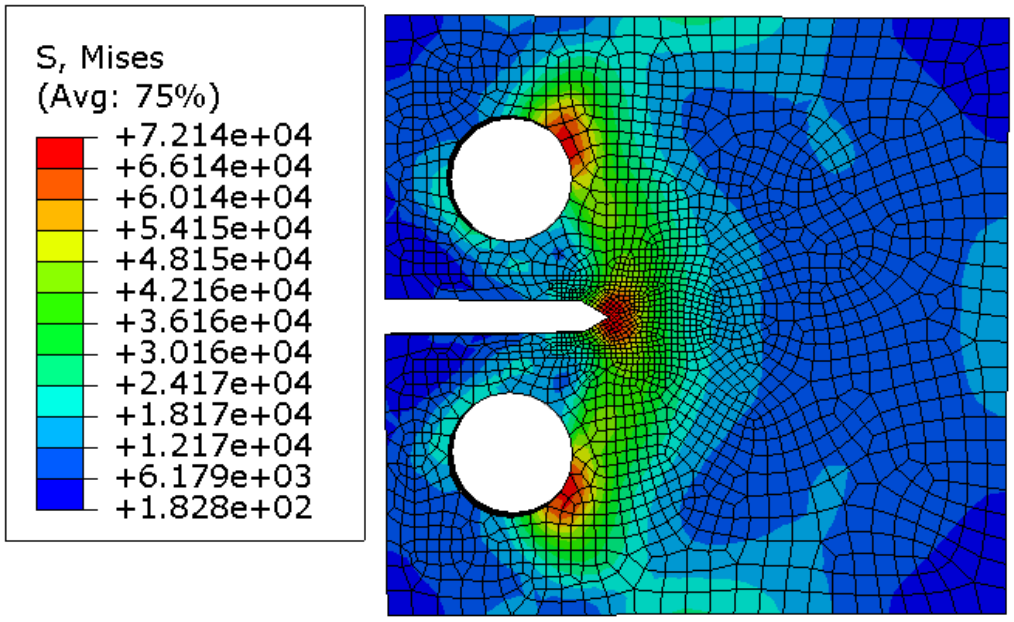

Figure 5.5 von Mises stress contours at first full loading (*t*=0.32).

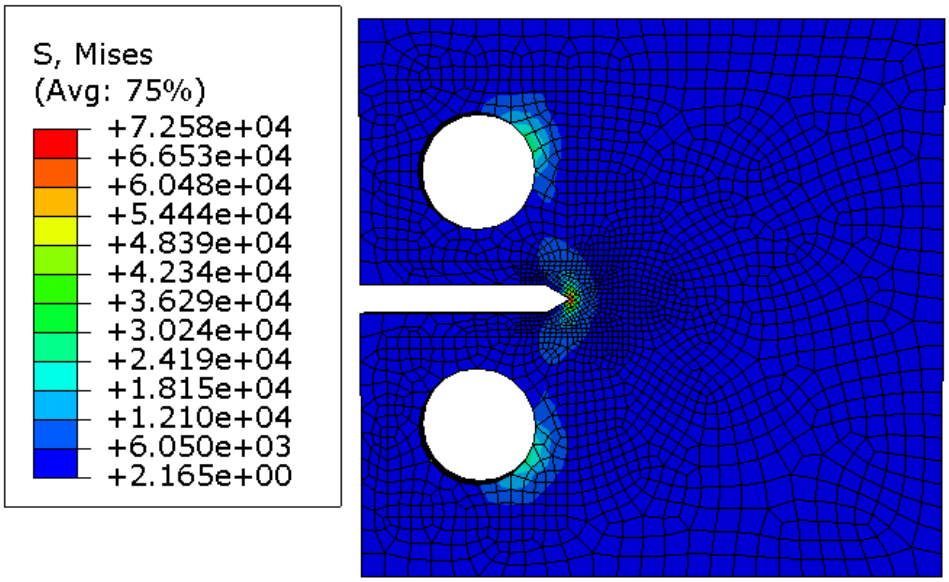

Figure 5.6 von Mises stress contours at full unloading (*t*=0.66).

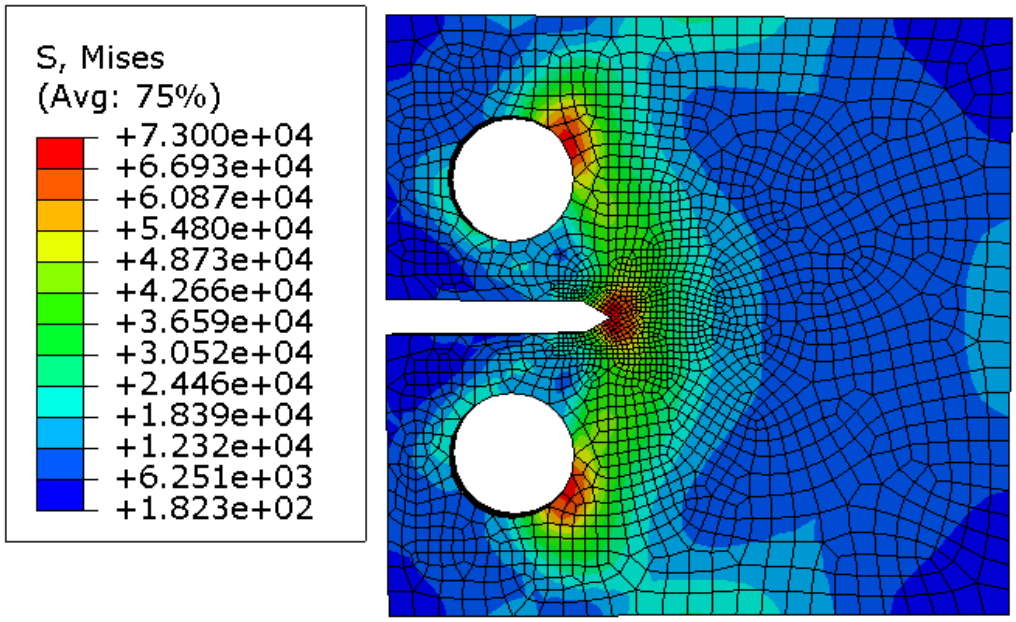

Figure 5.7 von Mises stress contours at second full loading (t=1.00).

The stress contours in Fig. 5.5 and Fig. 5.7 show that the shape of the stress contour for the part is consistent between the first loading and the reloading steps. The reaction force at the top pin due to the prescribed displacement is 2,016 lbf for both loading steps. However, the stresses for the reloading are generally about 2% higher on the second loading step than they were for the first loading step. The $\%_{Difference}$ convergence criteria for this model, calculated using Eqn. 3.1, was 0.43% based off the displacement at the submodel partition.

5.2.2 Quasi-Static Plastic Model Plastic Zone Validation

Figure 5.6 suggests that there is a plastic zone formation occurring in the area local to the crack tip when the part is completely unloaded. Figure 5.8 and Fig. 5.9 confirm this phenomenon.

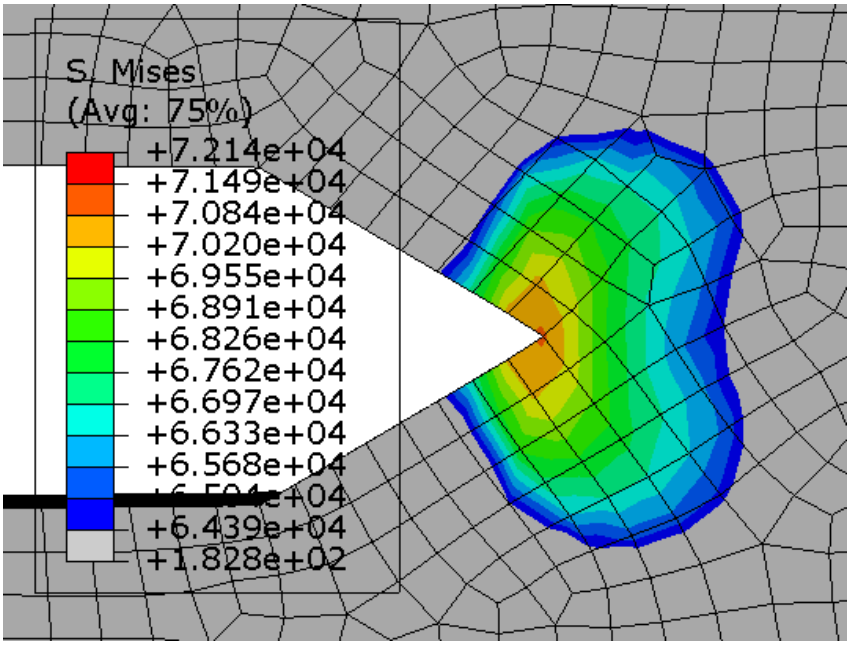

Figure 5.8 von Mises contour of stress with lower limit at material yield at the crack tip after one loading.

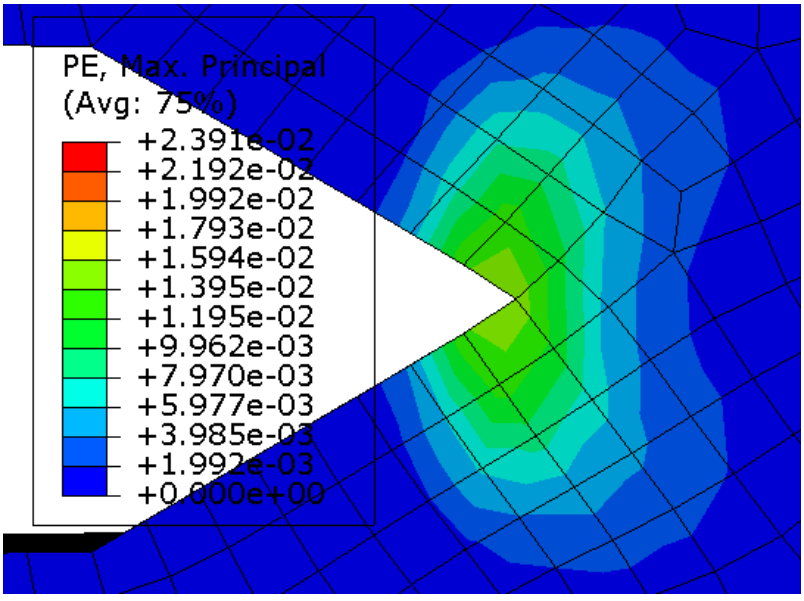

Figure 5.9 Contour of the plastic strain local to the crack tip after one load- unload cycle.

This plastic zone has a size of 0.157 inches when measured across the widest breadth of the plastic area from the plastic strain contour plot. This plastic zone size is consistent with the estimate of the plastic zone size from Dowling [3], Eqn. 5.1.

$$2r_{0\sigma} = \frac{1}{\pi}\left(\frac{K}{\sigma_0}\right)^2 \tag{5.1}$$

To use this equation, the K value is estimated from the reaction force at the pins and the closed-form stress intensity equation in Eqn. 3.2. The reaction force at the pins from the forced displacement is 2,016 lbf, which leads to a K value of 48.04 ksi$\sqrt{\text{in}}$. The yield stress for this material is 64.39 ksi based off the Ramberg-Osgood estimate at 0.2% plastic strain offset. The plastic zone diameter from the analytical estimate in Eqn. 5.1 is 0.177 inches. The plastic zone diameter estimate from the model value falls within 0.02 inches of the expected value from the closed-form analytical solution. This plastic zone is believed to be accurate and valid to use in proceeding steps.

Before proceeding to the fracture submodel portion of this analysis, it is important to determine if linear elastic fracture mechanics (LEFM) is valid to use for the compact specimen under this loading. To evaluate if linear elastic fracture mechanics is appropriate the inequality in Eqn. 5.2 must be satisfied.

$$a, (b-a), h \geq \frac{4}{\pi}\left(\frac{K}{\sigma_0}\right)^2 \tag{5.2}$$

The right side term of the inequality is determined using the stress intensity factor and yield stress discussed previously with Eqn. 5.1. The right side term is determined to be 0.452 inches which is greater than the initial crack length, *a*, for this model which is 0.4 inches. Therefore, linear elastic fracture mechanics are not valid for this analysis and subsequent steps will need to utilize the J-integral instead of using *K*.

Now that the validity of the model plastic zone properties are established and the limitations of linear elastic fracture mechanics are determined to be exceeded by this model, the submodel can be developed. This submodel will utilize the displacement field that the quasi-static model produced to generate a refined fracture model.

5.3 Development of Refined Fracture Submodel

A submodel is used to explore the area local to the crack front in this step. This modeling technique is necessary because running a fracture model of this size and mesh density with plasticity and a fracture singularity is computationally very expensive. The approach used to satisfy the elastic-plastic modeling objective was a two-model method with one quasi-static far-field displacement model and one fracture submodel. A restart analysis is not compatible with the needs of this analysis since the addition of the crack front singularity requires a remesh around the crack front with elements capable of representing the singularity. The displacement field cannot be imported as a predefined field or initial state for the fracture model because the mesh from the global quasi-static model overwrites the mesh in the fracture submodel. This mesh overwrite prevents the mesh from having the degeneracy at the crack tip. The submodeling technique is the best option for this analysis as it allows for a mesh change for the fracture model. In addition, the submodeling technique allows the geometry to be simplified to reduce the computational complexity by enforcing the displacement field on the simplified geometry boundaries.

5.3.1 Fracture Submodel Attributes

The first step in creating the submodel is to set the attributes in the model definition to read the job file from the quasi-static run. This is done under the submodeling attributes in the Abaqus model definition dialog window. The Abaqus dialog window for setting the submodeling attributes is shown below in Fig. 5.10.

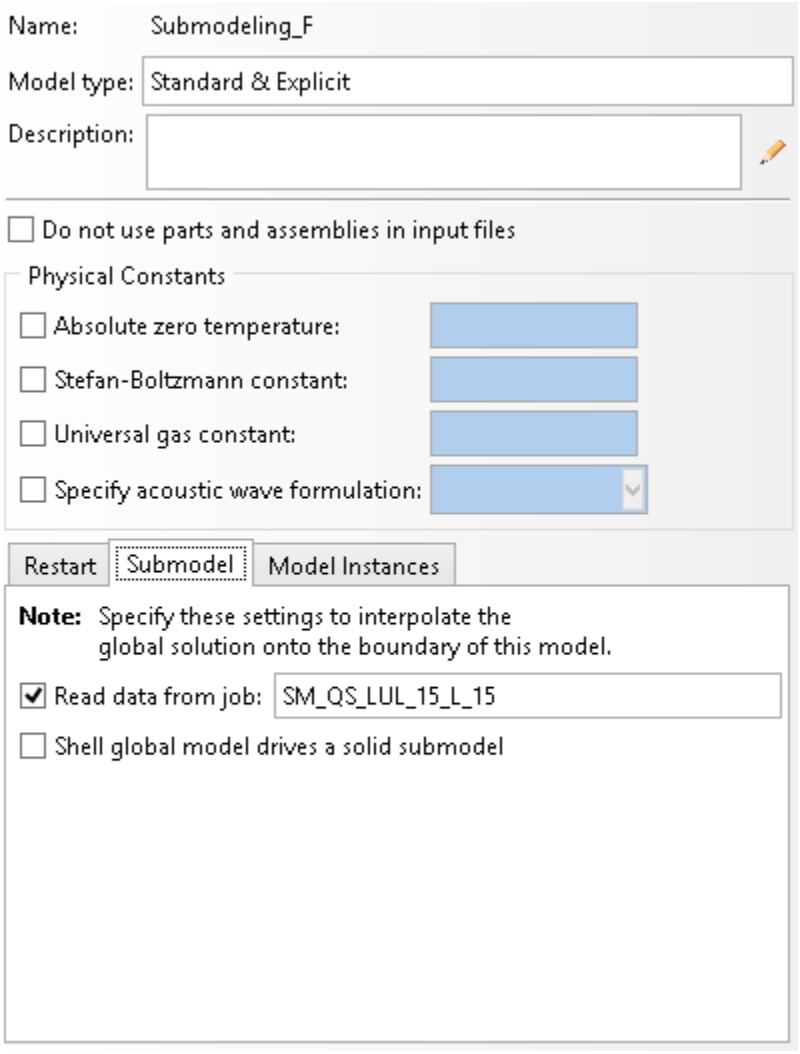

Figure 5.10 Submodeling attributes Abaqus dialog window.

5.3.2 Fracture Submodel Part, Partition, and Material

The part for the fracture submodel is defined by cutting the geometry from the quasi-static model at the partition around the crack tip area, which was previously used to generate the focus mesh in the crack tip region. Figure 5.11 shows the cut geometry for the submodel.

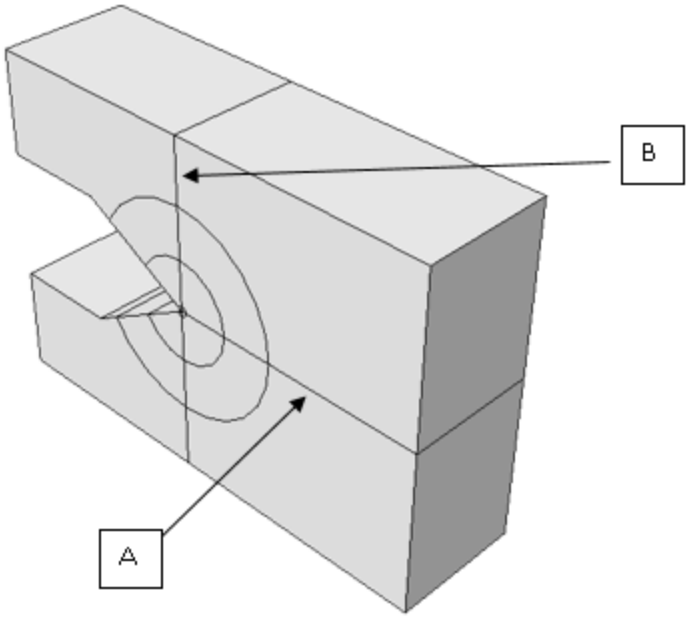

Figure 5.11 Cut submodel geometry for fracture analysis.

The partitioning strategy for the submodel is designed to generate the most effective mesh for capturing the fracture behavior. This behavior capture includes accurately representing the singularity and providing consistent elements from which to calculate the J-integral contours. The circular crack tip partitions have radii as defined in Table 5.3.

Table 5.3 Focus Area Partition Radii for Fracture Submodel

Partition	Radius (in)
R0	0.005
R1	0.05
R2	0.1

The circular partitions are further partitioned into 90-degree sections by two additional partitions that divide the entire submodel. One of the additional partitions creates a line of symmetry parallel to the top of the submodel geometry, Marker A in Fig. 5.11. The other

partition is parallel to the back face of the submodel geometry and intersects with the crack front, Marker B in Fig. 5.11.

The entire submodel geometry is assigned a section property that corresponds to the elastic-plastic Aluminum 7075-T651 material property as defined in Chap. 5.1. In the plastic region, this material behaves according to the Yield Strength-Plastic Strain pairs located in Table 5.1.

5.3.3 Fracture Submodel Crack Properties

The only interaction that is present in this submodel is the crack because the holes for the pin interactions are not included in the part region for this model. The crack front is located at the intersection of the two angled faces and the q-vector points towards the back face of the submodel geometry. The elements in contact with the crack front are degenerate elements that have a repeated node on the collapsed side. These degenerate nodes have the midside node positioned at 0.5 [1]. The Abaqus dialog window for setting the singularity properties is shown in Fig. 5.12.

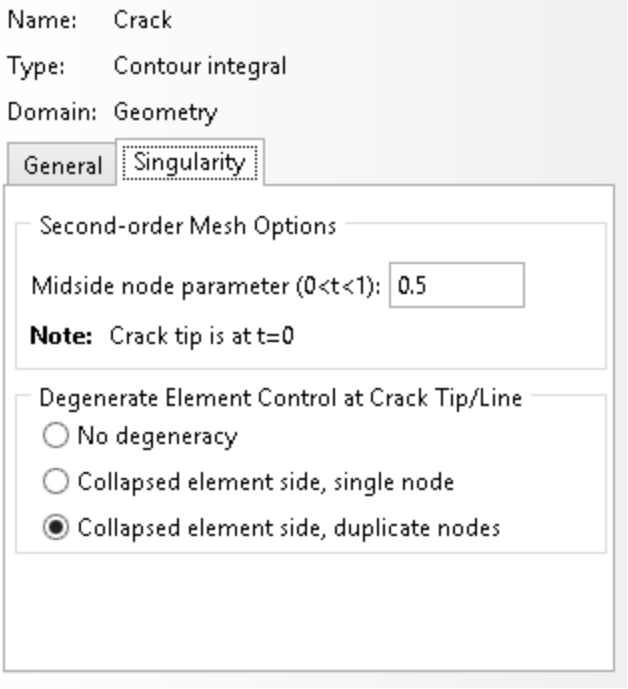

Figure 5.12 Abaqus singularity dialog window settings for elastic-plastic fracture.

The crack front, red edge with a green "X" at each end, and q-vector, blue arrows, are shown below in Fig. 5.13.

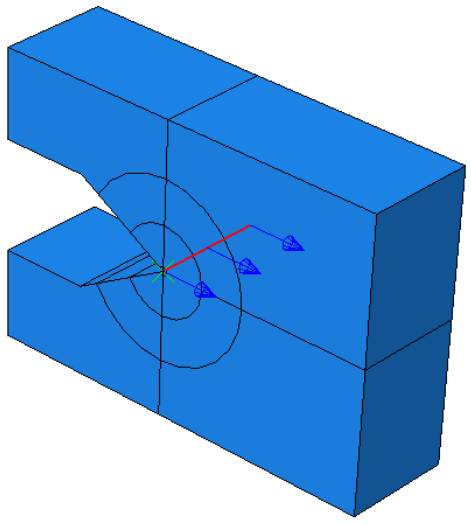

Figure 5.13 Crack interaction for submodel.

5.3.4 Fracture Submodel Boundary Conditions

The only load or boundary condition applied to the submodel is the submodeling boundary condition. The submodeling boundary condition applies the resulting displacement field of the quasi-static global model to the new surfaces created from cutting the submodel geometry out of the global model geometry. Figure 5.14 shows the faces where the displacement field from the global model is applied.

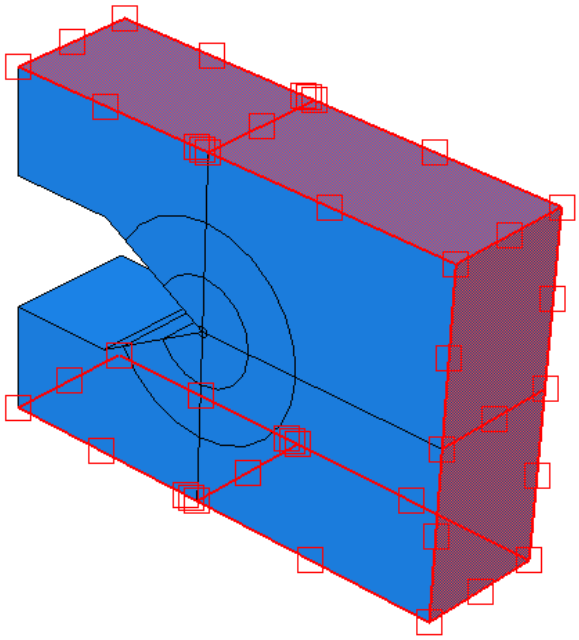

Figure 5.14 Boundary condition for submodeling applied to new surfaces.

This boundary condition applies the resultant displacement field of the nodes on the submodel surface from the global model to the nodes and elements in the submodel. This allows for the full Load-Unload-Reload cycle to be applied to the submodel using this one boundary condition. The submodel boundary condition uses only the displacements on the submodel surfaces in all three directions. The Abaqus property dialog window to set this boundary condition is shown in Fig. 5.15 below.

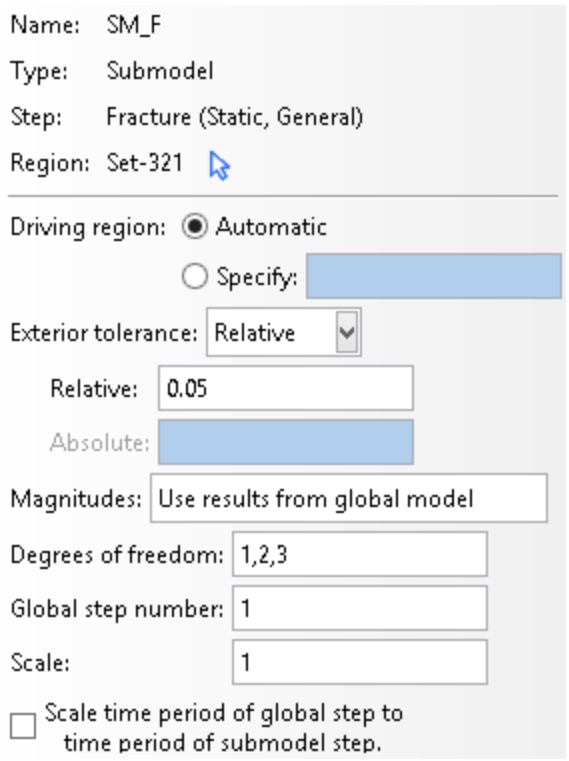

Figure 5.15 Abaqus dialog window for submodel boundary condition.

One significant downside to submodeling is that the fracture singularity (the submodel geometry containing the crack) must be present for all the iterations since the whole load cycle is performed on the submodel. The inclusion of the crack submodel geometry when building the plastic zone was determined to lead to insignificant changes in the size and properties of the plastic zone from dog bone prototype model runs.

5.3.5 Fracture Submodel Mesh

The circular partitions are seeded to have elements at exactly a 15-degree sweep angle. Additionally, the partitions that divide the circular partitions are seeded such that the element within the first circular partition is the smallest and the elements are gradually increased in size radially as they move away from the crack front. The elements in the circular crack front region are 20-node quadratic brick, hybrid, linear pressure, reduced integration elements (C3D20RH).

The degenerate elements at the crack tip are also of type C3D20RH since there are duplicate nodes on the collapsed side. The remainder of the elements are 8-node linear brick, hybrid, constant pressure, reduced integration, hourglass control elements (C3D8RH). These elements are utilized because they are finely meshed enough to appropriately transmit the prescribed displacement across the short distance from the edge where the boundary condition is applied to the focus mesh area. This saves on computational time while not sacrificing a significant amount of accuracy. The through-thickness direction mesh is a double biased mesh towards the center that has elements through the thickness. The bias towards the center was added to ensure the displacement field at the center did not rely on interpolations over large distances. The mesh size at the edges was verified to capture the edge behavior gradient before biasing was applied. Figure 5.16 below shows the mesh used for the fracture submodel.

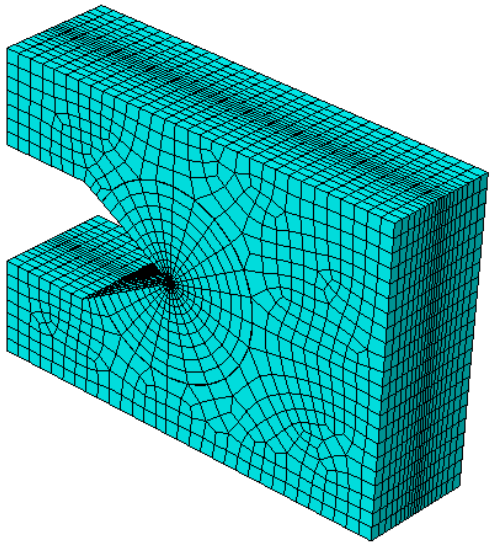

Figure 5.16 Fracture submodel mesh.

5.4 Results of the Refined Fracture Submodel

This section summarizes the results of the fracture submodel including stress at key time intervals and the J-integral.

5.4.1 Fracture Submodel Stress

A key aspect to ensuring that the submodel boundary condition is correctly transferred to the submodel from the global model is verifying the displacement at the boundary. The displacement field at the boundaries for the submodel matches the strain field at the partition in the global model. The stress at each step of the Load-Unload-Reload cycle can now be explored. Figure 5.17, Fig. 5.18, and Fig. 5.19 show the stress contours at each step in the load cycle.

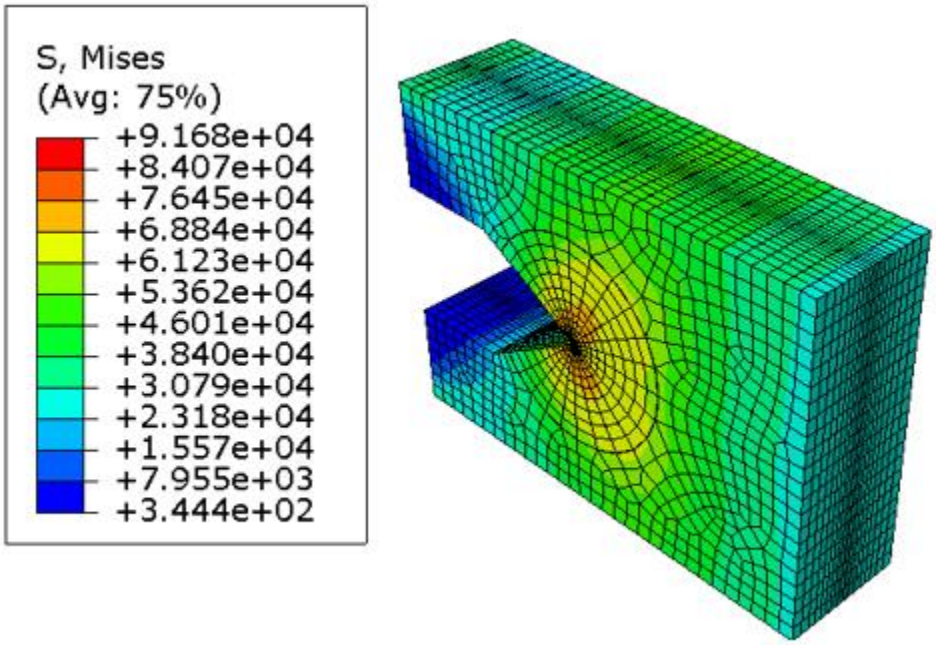

Figure 5.17 von Mises submodel stress contour plot for primary loading (t=0.32).

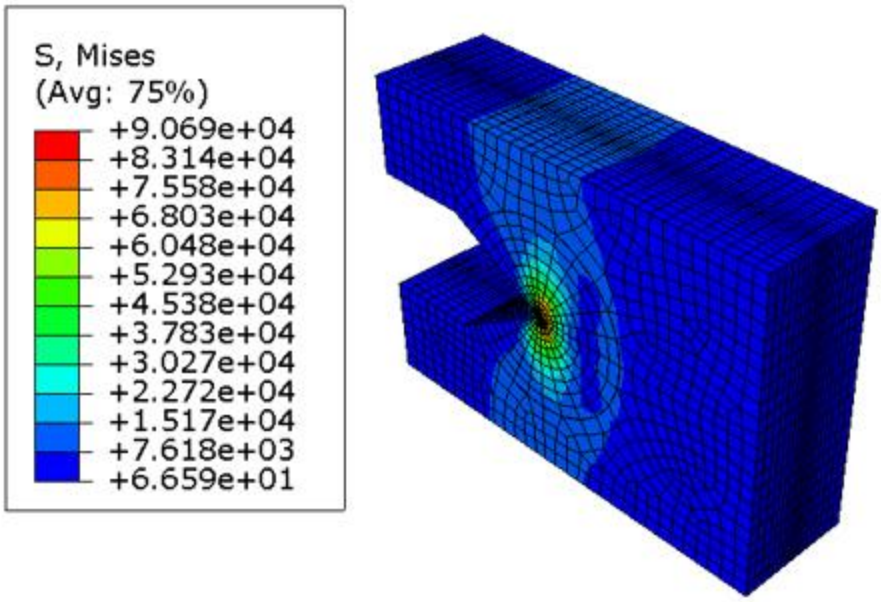

Figure 5.18 Submodel stress contour plot for unloading (*t*=0.66).

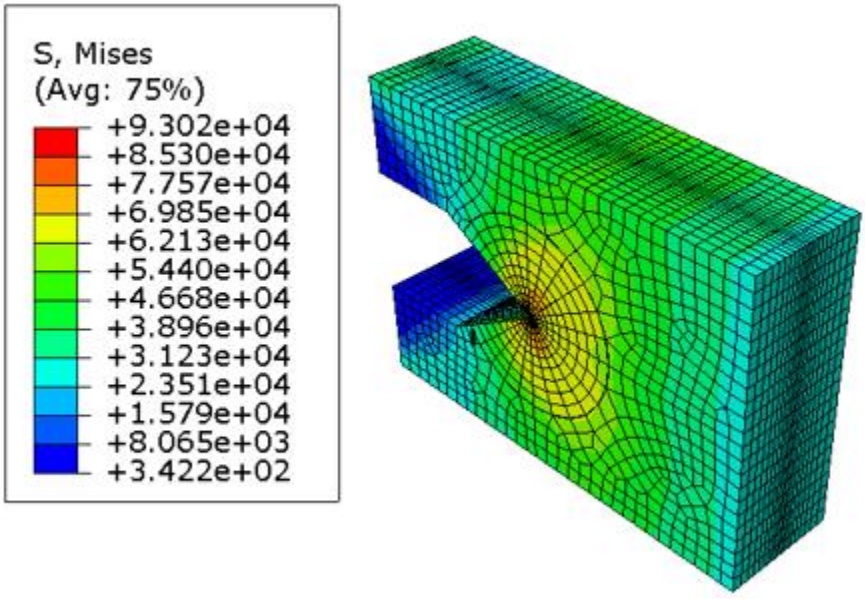

Figure 5.19 Submodel stress contour plot after reloading (*t*=1.00).

Similar to the quasi-static model, the stresses for the reload step increased 2% from the stresses for the first load step. Moreover, as shown in Fig. 5.20, the plastic zone after the unload step for the submodel is similar in size and shape to the plastic zone in the quasi-static model.

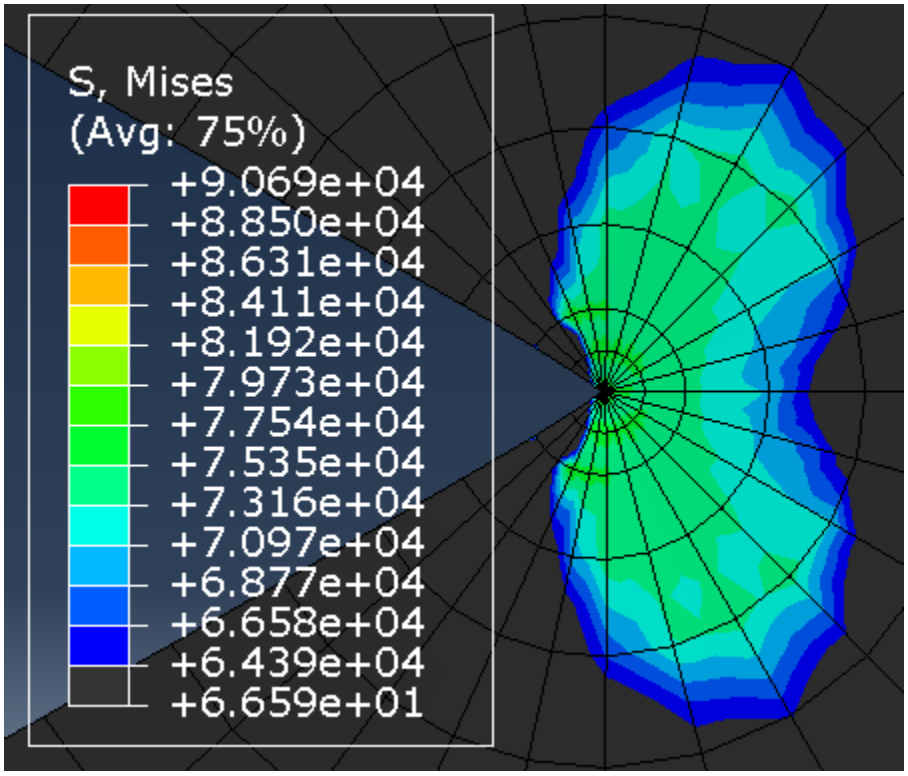

Figure 5.20 Submodel plastic zone after complete unloading.

5.4.2 Fracture Submodel J-integral

For this model, the J-integral at the completion of the last loading (t=1.00) was 159.5 [psi-in] which had the second through fifth contour integrals all within 3.5% of each other. The $\%_{Difference}$ convergence criteria for this model, calculated using Eqn. 3.1, was 0.66% based off the J-integral. The J-integral for the fracture submodel on the first load step was 131.75 [psi-in], which was a 3.75% increase from the J-integral for the first loading of the three-dimensional linear elastic fracture mechanics model. The reload step J-integral, 159.5 [psi-in] was an 18%

increase from the first load step. This demonstrates that the model is replicating a realistic change in J-integral with additional reloading of the residual stress zone.

6. Summary, Conclusions, and Future Work

This section will summarize the work done during, state the conclusions from, and discuss ideas for future work building on this research.

6.1 Goals and Objectives

The research goals stated in Chap. 1.3 provided a framework for the progression of this research project. The primary goal of this research was to develop a finite element modeling technique that robustly modeled the stress intensity, as it related to crack initiation, in plastic zones. To achieve this main goal, many other models including two and three-dimensional linear elastic models and a variety of supplemental dog bone models had to be developed. The explicit objectives for obtaining these goals are:

1. Linear elastic fracture mechanics (LEFM) models were created in two and three dimensions, techniques validated were then used later in the elastic-plastic fracture mechanics models,
2. The two and three-dimensional LEFM models were validated with closed-form solutions to 6% and 0.57% respectively,
3. Dog bone models were completed for submodeling methods, singularity impact, and model elastic-plastic response verification,
4. The plastic zone local to the crack tip was modeled in the quasi-static global model,
5. The plastic zone was transferred from the quasi-static global model to the fracture submodel,

6. Elastic-plastic fracture mechanics in a residual stress zone was modeled in the fracture submodel.

6.2 Summary of Completed Work and Conclusions

This study achieved the goal of iteratively generating a residual stress state model that was analyzed for fracture during a Load-Unload-Reload cycle. This goal was accomplished by first generating a two-dimensional linear elastic model for fracture initiation using a plane strain material model. The next phase developed a linear elastic model in three dimensions and the stress intensity properties were once again determined. Finally, plasticity was added to the model and the load cycle was updated such that a plastic zone was formed in the region local to the crack tip. This model was run only in the quasi-static state so that the far-field stress state could be used as the global model for a fracture submodel. The fracture submodel was generated to determine the J-integral, a fracture initiation property for elastic-plastic fracture mechanics.

The two and three-dimensional linear elastic models were able to verify the meshing methodology and the modeling technique. The techniques developed in the linear elastic models were used in the elastic-plastic quasi-static global model and fracture submodel. The linear elastic models were verified against closed-form solutions. The two-dimensional model was found to have 6% error. The three-dimensional model had less than a 1% error off the closed-form solution. The plastic zone from the plasticity model also fell within 0.02 inches of the estimate for plastic zone diameter in the estimate [3]. The quasi-static global model was verified to be outside the limitations of linear elastic fracture mechanics. The fracture submodel run produced a J-integral value that represented the crack initiation property that was within the acceptable range.

This research explored using the deformation plasticity equation as a Ramberg-Osgood material law. However, Abaqus only intends for deformation plasticity laws to be used with monotonic loading. Instead, a tabulated plastic stress-strain response had to be defined to establish the elastic-plastic material response. Dog bone models were developed to ensure that the material properties in Abaqus accurately produced the stress-strain behavior for the part.

The elastic-plastic fracture analysis proved to be a much more sensitive analysis than the linear elastic predecessors. The fracture submodel required more mesh refinement to prevent element distortion at the crack tip and to produce converged contour integrals. Submodeling allowed for faster iterations of the mesh, which allowed for more mesh schemes to be attempted.

Utilizing a submodel for the fracture step is the best Abaqus method for this problem. Submodel analysis requires that the fracture singularity had to be present during the development of the plastic zone. Ideally, the model would form a plastic zone without the fracture singularity present then the singularity would be added into the model solely for the reload step where fracture data is gathered. Abaqus does not support this type of model update. Other methods that proved to be inadequate for this model include importing the plastic zone as an initial state predefined field and running a restart analysis. Neither of these methods allowed for the fracture singularity to be added to the mesh since the mesh used for the global quasi-static model had to be carried through to the second step where the fracture would theoretically be added.

The research conducted through these models is useful because the techniques required to adequately model a fracture in a plastic zone are defined. This could prove to be useful in industries, such as aerospace, that evaluate failure based on fracture. One application of this type of modeling would be for additive metal manufacturing applications. The underlying process of forming a plastic zone then performing fracture analysis on that part could be applied to the additive manufacturing model as well. This research could serve as a starting point for a deeper exploration of elastic-plastic facture modeling in plastic zones where there is a large depth of research potential. The methodologies developed in this research are still early in their development and still require a large amount of future work to bring them to their full potential.

6.3 Future Work

Finite element modeling of fracture mechanics in residual stress zones is a topic that is in the early stages of development and exploration. This section is dedicated to discussion of areas in which this research can be improved, expanded, and applied

6.3.1 Future Model Improvements

.

The model should undergo much further research in the area of optimizing the techniques that go into creating the model. The first study that should be conducted to improve this research is performing experiments to aid in the validation of the elastic-plastic fracture models. Feedback on the experimental set-up will need to be provided to the model so parameters, like friction between the pins and specimen, are properly represented. Examples of research that could be done once the experimental data is generated include sensitivity analyses to the model parameters. More work should be done in determining the ideal size of the focus mesh around the crack tip and determining the most viable crack tip mesh density. Element order, shape, and integration schemes should also be explored and optimized as a future step of this research. Different meshing schemes, including different midside node adjustments, should be systematically tested to determine the J-integral sensitivity to the change in those parameters. Work should also be done to verify that the same results are obtained using different versions of the Abaqus solver. Another sensitivity analysis that should be conducted is determining the size of and features included in the submodel. These additional research items could further improve the robustness of the model and marketability as a method for use in industry applications.

6.3.2 Expanded Capability to the Research

Another potential direction for this research would be determining stress intensity factor in the plastic zone throughout several cyclic runs. This experiment could determine how the stress intensity factor is directly affected by the growth and intensity of the plastic zone. This

could be done by modifying the existing model's load amplitude function to incorporate more load cycles. This model could be used as a method of virtual testing to determine the change in the stress intensity factor as a function of number of load cycles or as a function of load amplitude. Another way this model could be utilized in a virtual testing application would be to incorporate the extended finite element method (XFEM) to model how crack growth occurs through areas with preexisting plastic zones. These virtual crack growth studies could have as much value in industrial applications as the crack initiation study in this research. This research could also be expanded into blunt crack fronts as well. Adding the blunt crack functionality would likely result in changes to the meshing strategy but very few adjustments in other aspects of the model.

6.3.3 Additional Applications for this Research

This research could be used to explore further specific applications such as thermal residual stress modeling to determine residual stresses in specific metal additive manufacturing processes. Thermal gradient modeling methods are useful when modeling the additive manufacturing process since most additive manufacturing processes heat the material. This investigation could determine methods for printing to optimize properties such as overall part resistance to fracture. This information could be utilized in the machine print orientation automatic optimization process. This property could be balanced with print time and support material costs to determine the optimal orientation. Another opportunity to use the modeling technique is to determine the stress intensity factor around a hole with an interference fit. Interference fits are known to generate a plastic zone and be susceptible to fracture.

References

[1] Dassault, “Classical Fracture and Failure in Abaqus.” 2011.

[2] V. Cain, L. Thijs, J. V. Humbeeck, B. V. Hooreweder, and R. Knutsen, “Crack propagation and fracture toughness of Ti6Al4V alloy produced by selective laser melting,” Additive Manufacturing, vol. 5, pp. 68–76, 2015.

[3] N. E. Dowling, Mechanical behavior of materials: engineering methods for deformation, fracture, and fatigue, 4th ed. Hoboken, NJ: Pearson Education, Inc., 2019.

[4] R. M. McMeeking, “Finite Deformation Analysis of Crack-Tip Opening in Elastic-Plastic Materials and Implications for Fracture,” Journal of Mechanical Physical Solids, vol. 25, pp. 357–381, 1977.

[5] R. Barsoum, “On the Use of Isoparametric Finite Elements in Linear Elastic Fracture Mechanics,” International Journal for Numerical Methods, vol. 10, pp. 25–37, 1976.

[6] R. Barsoum, “Triangular Quarter Point Elements as Elastic and Perfectly Plastic Crack Tip Element,” International Journal for Numerical Methods, vol. 11, pp. 85–98, 1977.

[7] S. Suresh, “Elastic-Plastic Fracture Mechanics.”

[8] R. M. McMeeking, “Finite Deformation Analysis of Crack Tip Opening in Elastic-Plastic Materials and Implications for Fracture Initiation,” Jan. 1976.

[9] American Society for Testing and Materials, “Standard Test Method for Plane-Strain Fracture Toughness of Metallic Materials1.” 1997.

[10] “Abaqus/CAE User's Guide (6.13),” Conversion Tables, Constants, and Material Properties. [Online]. Available: http://abaqus.software.polimi.it/v6.13/books/usi/default.htm?startat=pt03ch11s07s01.html.

[11] "Aluminum 7075-T6; 7075-T651," ASM Material Data Sheet. [Online]. Available: http://asm.matweb.com/search/SpecificMaterial.asp?bassnum=MA7075T6.

[12] "Friction and Friction Coefficients," Densities of Solids. [Online]. Available: https://www.engineeringtoolbox.com/friction-coefficients-d_778.html.

Appendix A: Ramberg-Osgood Material Law

Ramberg-Osgood approaches are preferred because one continuous function is produced. Unless Ramberg-Osgood constants are available for the material of interest, the constants must be calculated from experimental data. The first step to calculating Rambeg-Osgood constants is calculating the plastic strain (ε_p) for each data point according to Eqn. 2.3

$$\varepsilon_P = \varepsilon - \frac{\sigma}{E} \tag{A.1}$$

In Eqn. A.1, ε is the total strain, E is the Young's Modulus, and σ is the stress. This equation solves for the plastic strain by subtracting the elastic strain from the total strain. The second step to producing Ramberg-Osgood constants is to plot all the data points that have significant plastic strains, and therefore are in the plastic region, according to Eqn. A.2.

$$\log \sigma = n \log \varepsilon_P + \log H \tag{A.2}$$

The new variables in this equation are defined as follows, n is a constant that is rooted in the general slope of the plastic region and H is the stress when $\varepsilon_P = 1$. The third step to calculating the Ramberg-Osgood constants is to apply a linear best-fit line to Eqn. 2.4. The resulting conversions from the linear fit in the form of $y = mx + b$ are: $y = \log \sigma$, $x = \log \varepsilon_p$, $m=n$, and $b = \log H$. Once these constants are solved, the equation can be used in the Ramberg-Osgood form shown in Eqn. A.3 [3].

$$\varepsilon = \frac{\sigma}{E} + \left(\frac{\sigma}{H}\right)^{\frac{1}{n}} \tag{A.3}$$